UNIVERSITI PUTRA MALAYSIA

ELECTROMAGNETIC INDUCTION ABSORBANCE OF POLT(ETHYLENE TEREPTHALATE)-CARBON NANOTUBES (PET-CNTs) NANOCOMPOSITES

NUR HAMIZAH BINTI HASHIM

ELECTROMAGNETIC INDUCTION ABSORBANCE OF POLT(ETHYLENE TEREPTHALATE)-CARBON NANOTUBES (PET-CNTs) NANOCOMPOSITES

By

NUR HAMIZAH BINTI HASHIM

Thesis Submitted to the Department of Physics, Universiti Putra Malaysia, in partial Fulfilment of the Requirements for the Degree of Bachelor of Science in Materials Science with Honours

February 2022

DEDICATION

This thesis is dedicated to

My beloved supervisor *Dr Md Shuhazlly Mamat*

My parents *Hashim Asran* and *Zainab Sitam*

My project coordinator *Nurul Fatihin Izatil Azman* and *Chan Kar Fei*

My lecturers,

My siblings,

My friends,

and others who help me through the completion of this thesis.

ABSTRACT

Electromagnetic Induction Absorbance of PET-CNTs Nanocomposite

by

Nur Hamizah Binti Hashim

198940

February 2022

Supervisor: Dr. Md Shuhazlly Mamat

Faculty: Faculty of Science

The aim of the research is to determine the EMI absorbance of PET and PET nanocomposite with carbon nanotubes nanofillers at two different compositions which is 0.1 wt.% and 0.5 wt.%. The polyethylene terephthalate (PET) was manufactured in this study using melt blending and injection molding with the addition of different carbon nanotubes (CNTs) fillers. The structure and morphology of the fabricated PET-CNTs nanocomposites were determined using a field emission scanning electron microscope (FESEM), and the nanocomposites phases were interpreted using X-Ray Diffraction (XRD). The electrical properties and the materials' EMI absorbance behavior can be determined using the two-point probe method and Vector Network Analyzer (VNA). FESEM demonstrates that when the filler composition increases, the structures and morphologies of the nanocomposites become more visible. Carbon nanofiller was shown to improve the electrical conductivity and EMI absorption of polymer nanocomposites.

ABSTRAK

Induksi Penyerapan Elektromagnet terhadap nanokomposit

oleh

Nur Hamizah Binti Hashim

198940

Februari 2022

Penyelia: Dr. Md Shuhazlly Mamat

Fakulti: Fakulti Sains

Tujuan penyelidikan ini adalah untuk mengkaji penyerapan elektromagnetik induksi terhadap PET dan PET nanokomposit dengan komposisi karbon tiub nano yang berbeza iaitu 0.1 pb% dan 0.5 pb%. Dalam penyelidikan ini, Poli(etilena Terephthalate) (PET) telah disediakan dengan menggunakan kaedah pencairan campuran dan pengacuan suntikan dengan penambahan karbon tiub nano (CNT). Morfologi nanokomposit PETCNT yang dianalisis mengunakan Mikroskop Elektron Pengimbasan Pelepasan Lapangan (FESEM) manakala Difraksi Sinar-X (XRD) menunjukkan fasa nanokomposit. Untuk menentukan sifat elektrik dan tingkah laku penyerapan induksi elektromagnetik bahan, kaedah kekonduksian dua titik dan penganalisis rangkaian vektor (VNA) digunakan. FESEM menunjukkan bahawa struktur dan morfologi nanokomposit lebih kelihatan apabila komposisi pengisi meningkat. Kehadiran pengisi karbon meningkatkan kekonduksian elektrik dan penyerapan gelombang mikro ke atas polimer nanokomposit tersebut.

ACKNWOLEDMENT

First and foremost, praise and gratitude to the presence of the Almighty God, for by His bounty I was able to complete this study successfully. The success and completion of this project requires extensive guidance and assistance from many people. I was very fortunate to receive this in addition to completing my research and thesis preparation. I have achieved everything solely because of such supervision and help, and I will never forget to say thank you.

I am indebted to my supervisor, Dr. Md Shuhazlly Mamat, for all his support and guidance in ensuring I completed this project successfully. I am indebted to him for his guidance and willingness to provide feedback throughout this research, even though he has a busy schedule for these two semesters.

I would like to express my deepest appreciation to my postgraduate seniors Nurul Fatihin Izatil Azman and Chan Kar Fei, my friends Raja Hazwani and Fatin Nadhirah for their encouragement, immediate support, and guidance throughout the duration of my project work by providing all thenecessary information.

I would like to thank all the technicians and staff of the Department of Physics and the Institute of Tropical Forestry and Forest Products (INTROP) at UPM for their guidance in completing my project work. In addition, I would like to record my thanks to all my friends who contributed, taught, and assisted me in completing this thesis.

APPROVAL

*This thesis entitled "***Electromagnetic Induction Absorbance of PET-CNTs Nanocomposite***" by Nur Hamizah Binti Hashim (Matric No.: 198940) was submitted to the Department of Physics, Faculty of Science, Universiti Putra Malaysia and has been accepted as partial fulfillment of the requirement for the Bachelor of Science in Materials Science with Honours.*

Approved by,

Date: 07/08/2022 ……

Dr. Md Shuhazlly Mamat
Project Supervisor
Department of Physics
Faculty of Science
Universiti Putra Malaysia

Date : ……

Dr. Md Shuhazlly Mamat
Course Coordinator
Department of Physics
Faculty of Science
Universiti Putra Malaysia

Date: ……

Assoc. Prof. Dr. Suriati Paiman
Head of Department
Department of Physics
Faculty of Science
Universiti Putra Malaysia

DECLARATION

Declaration by student

I hereby confirm that:

- this thesis is my original work;
- quotations, illustrations and citations have been duly referenced;
- this thesis has not been submitted previously or concurrently for any other degree at any other institutions;
- intellectual property from the thesis and copyright of thesis are fully owned by Universiti Putra Malaysia, as according to the Universiti Putra Malaysia (Research) Rules 2012;
- written permission must be obtained from supervisor and the office of Deputy Vice-Chancellor (Research and Innovation) before thesis is published (in the form of written, printed or in electronic form) including books, journals, modules, proceedings, popular writings, seminar papers, manuscripts, posters, reports, lecture notes, learning modules or any other materials as stated in the Universiti Putra Malaysia (Research) Rules 2012;
- there is no plagiarism or data falsification/fabrication in the thesis, and scholarly integrity is upheld as according to the Universiti Putra Malaysia (Research) Rules 2012.

Signature: 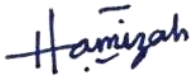 Date: 05 August 2022

Name and Matric No.: NUR HAMIZAH BINTI HASHIM (198940)

TABLE OF CONTENTS

LIST OF FIGURES

LIST OF TABLES

LIST OF ABREVIATIONS

CF	Carbon Filler
CNTs	Carbon Nanotubes
EM	Electromagnetic
EMI	Electromagnetic Interference
FESEM	Field Emission Scanning Electron Microscope
Mm	Millimeter
MWCNT	Multi-Wall Carbon Nanotubes
Nm	Namometer
NC	Nanocomposite
PET	Polyethylene Terephthalate
PNC	Polymer Nanocomposite
SE	Shielding Effectiveness
SWCNT	Single-Wall Carbon Nanotubes
VNA	Vector Network Analyzer
Wt.%	Weight Percent
XRD	X-Ray Diffraction

CHAPTER 1: INTRODUCTION

1.1 Background of Study

Polymers means “many parts” in Greek work and each of those parts is known as monomer which means “one part” in Greek. Polymers are molecules that have long sequences or chains of one or more species of atom or group of atoms that are bound together by a primary, normally covalent bond. Polymers is a broad concept that covers a diverse range of synthetic or semi-synthetic materials used in a wide variety of applications. The first plastics were made by nature and interest in producing plastics emerged in the 1800s as a way to replace scarce materials like ivory and tortoise shells. It is a polymeric substance that can be formed or shaped through the application of heat and pressure. Plastics can be made into a wide variety of products due to their often-combined special properties such as low density, low electrical conductivity, transparency, and hardness (Rodriguez et al., 2003).

Polymers can exist in natural polymers and synthetic polymers. For example, synthetic polymers are plastic and natural polymers are rubber and wood. Natural polymers usually consist of simple hydrocarbons and isoprene. Polymers have been used in many applications for years. It can be found in the clothing, the homes we live in, automobiles, toys, screens, IT instruments, and the medical equipment.

PET is an abbreviation for polyethylene terephthalate, a thermoplastic polymer that is a part of the polymer family. Polyester resins are best known for their exceptional mix of mechanical, thermal, chemical, and dimensional stability. PET is a semi-crystalline resin that, in its natural state, is extremely flexible, colorless, and semi-crystalline. It ranges in stiffness from semi-stiff to stiff, depending on the preparation

method. It has a high degree of dimensional stability, resistance to impact, moisture, alcohol and solvents.

Nanocomposites (NCs) are materials with many phases, one of which is nanoscale (Jeon & Baek, 2010). Polymers nanocomposite materials have generated considerable interest in academic and commercial research because they imply practical methods for improving the physical properties of conventional polymers, such as thermal stability, mechanical properties, decreased vapor permeability, and flame retardant properties (Mallakpour & Behranvand, 2017). By incorporating a small amount of carbon nanotubes (CNTs) into the polymer matrix, these polymer composite materials' electrical, mechanical, and thermomechanical properties can be enhanced (González et al., 2016) because of their high aspect ratio (greater than 1000), strength, and stiffness (133) (Mallakpour & Behranvand, 2017).

This research study investigates the utilization of carbon fillers, which is CNTs as microwave adsorption reinforcement in PET matrices. Microwave absorbers are being developed in both military and civilian applications to reduce radar signatures of aircraft, ships, and targets, as well as to reduce electromagnetic interference (EMI) between components and circuits (Qin & Brosseau, 2012). Carbon nanotubes are a promising application in the field of polymer-based nanocomposites, where they serve as an excellent reinforcing material due to their light weight and superior mechanical, thermal, and electrical properties (Cruz-Delgado et al., 2014).

Electromagnetic radiation is reflected and absorbed by a substance that acts as a shield against its penetration is known as Electromagnetic Interference Shielding. Electromagnetic interference (EMI) occurs when an electromagnetic field interferes with the operation of an electronic device. It typically occurs when the device is in

direct range to an electromagnetic field that causes the radio frequency spectrum to be disrupted. Radio-frequency interference is another term for this (RFI). Electromagnetic absorbance occurs when the electromagnetic waves strike a substance, the waves weaken, and energy is lost due to heat loss (Mohammed et al., 2019). The amount of energy emitted is mostly determined by the wave frequency and value, as well as the material's permeability and permeability (Mohammed et al., 2019).

There are few importance of EMI shielding especially to electronic devices. It isolates a device's energy so that it has no effect on other devices and prevents external energy from entering. As a result, if each one is properly insulated, they cannot interfere with one another. Without shielding, electronics would perform poorly or perhaps fail to function entirely. EMI shielding is important because it can prevent Brownouts and Blackouts. Brownouts are any form of partial service interruption, whereas blackouts are complete service interruptions. Brownouts and blackouts are not limited to outages caused by power failures. Following that, it is necessary to avoid Electrical Fast Transitions, or EFTs. If a power outage occurs while a transfer sequence is in place, power will be supplied by a generator. When this occurs, it is referred to be an EFT. If an EMI shielding is present, the device may receive unjustified EFTs. Additionally, static on phone line is one of the importance of EMI shielding. When the plastic jacket of a phone line is removed, a second layer concealing the wires is appearing. This second layer is typically a metallic foil or metallic plaited braid that shields the lines from electromagnetic interference (EMI). It is a sort of radio frequency shielding that helps eliminate static during phone calls. EMI shielding is also important in the event of a power failure. Any abnormality in an electrical current is referred to as a power fault. A short circuit is the best example

of a power failure, but it is not the only cause because Electromagnetic interference (EMI) can occasionally cause power failure.

1.2 Problem Statement

Electromagnetic absorbance behavior with a broad absorption bandwidth, lightweight, and cost-efficiency are expected in materials with excellent electromagnetic absorption (Qin & Brosseau, 2012). Carbon-based materials are best known for their unique properties, including superior electrical and mechanical properties that lead to excellent capabilities especially for EMI shielding. It was discovered that the electrical conductivity, permittivity, permeability, and structure of the shielding material all play a significant role in achieving excellent EMI shielding, and thus the balance of these properties is critical. (Gupta & Tai, 2019). Carbon nanoparticles have excellent electrical conductivity. Carbon black (CB), carbon fibres (CF), carbon nanotubes (CNTs), graphene nanosheets, and reduced graphene oxide (RGO) are all examples of carbon-based materials. There are many research in establishing high performance of polymers nanocomposite by merging PET with other substances. To create high-performance nanocomposites, the fillers must possess unique electrical, thermal, and mechanical properties. Carbon nanotubes were chosen as the fillers in this study.

CNT fillers can compensate for PET's limitations, such as poor mechanical characteristics and thermal stability. Despite their unique features, CNTs are occasionally spared from aggregation and poor distribution as reinforcement particles. By encapsulating the triangular lattice structure of the CNTs, van der Waals and the Coulomb forces attract the accumulated CNTs into groups (Gbaguidi et al., 2019). Aggregation of CNTs alters the size and distribution of filler particles, lowering the

aspect ratio. Furthermore, the CNTs mixture ratio can lower the percolation threshold and increase composite material performance.

1.3 Objective of Study

The aim of this research is to investigate the electromagnetic absorption of pure PET and PET-CNT nanocomposites. The specific objectives are:

I. To characterize and analyze the behavior of the pure PET and PET-CNTs nanocomposite with different composition of 0.1 wt% and 0.5 wt% to the Electromagnetics Interferences Absorbance.

II. To study the surface morphology of polymer nanocomposites, as well as the electrical properties of PET matrix when filled with different types of carbon nano-fillers.

1.4 Thesis Overview

This thesis is divided into five chapters, each of which describes the theories, methods, characterizations, and the results of the experimental investigation that was completed. In the first chapter is an introduction to this research field study. This chapter more focuses on the research background, problem statement, objectives, and overview of the overall thesis. In chapter 2, literature review is elaborated and describes in depth the rationale for the research study, as well as the characteristics of the main components of the study. This chapter also discuss the theory underlying the characterization processes and methods. The approach or procedure of the

research is described in the third chapter. This chapter also explain about the mechanism of the characterization and the formula needed for each concept. Without summarizing, the full research process is detailed, including raw materials, machines utilized, and experimental analyses. Chapter four contains the results and explanation of the investigations, including the influence of the electrical properties and characteristics of the samples. In the last chapter, which is chapter five, is important since it contains a summary of this study and suggestions for future research based on this thesis.

CHAPTER 2: LITERATURE REVIEW

2.1 Nanomaterials

Nanomaterials are defined as "materials with any outward dimension on the nanoscale or with an internal or surface structure on the nanoscale," with the nanoscale referring to lengths between 1 and 100 nm. Nanomaterials can be found in nature or synthesized as a by-product of combustion reactions, or they can be engineered to perform a specific function. These materials' physical and chemical properties may differ from those of their bulk-form equivalents. The features, particularly their size, provide a variety of benefits, and their adaptability in terms of the ability to customize them for specific applications increases their utility even further. When the size of a substance is reduced to the nanoscale, it is possible for the same material to exhibit completely different properties such as a different melting point, conductivity, and so on. This is because matter at the nanoscale violates Newtonian laws. Composites composed of nanoscale ceramics or metals with a diameter of less than 100 nanometers can unexpectedly become significantly stronger than current materials science models predict. Nanomaterials have a greater surface area when compared to the same mass of material produced in a larger form. Nanoparticles have the ability to alter a material's chemical reactivity, as well as its strength and electrical properties. Another advantage is their high porosity, which increases demand for their use in a variety of sectors.

Nanomaterials' high surface-to-volume ratio makes them particularly helpful in a variety of fields, including biomedical, industrial, electronics, renewable energy, health care, the environment, textiles, and food agriculture due to their capacity to create materials in a precise way to perform a specified purpose. Nanomaterials' size,

form, high reactivity, and other unique traits make them potentially advantageous in product development, but they also raise concerns about the nature of their interaction with biological systems and potential environmental impacts. Nanomaterials are beneficial in the energy sector because they have the potential to increase the efficiency and cost-effectiveness of conventional energy generation systems, such as solar panels, as well as provide new methods for energy collection and storage. They are also expected to benefit the electronics and computer industries in a variety of ways. Their use will enable greater atomic-level precision in the construction of electronic circuits, allowing for the creation of a broader range of electronic devices.

2.2 Nanocomposites

A composite is a structural material composed of two or more coupled elements that are not macroscopically soluble in one another. The reinforcing phase is one of the constituents, while the matrix is is the one in which it is embedded. Reinforcing phase materials can be fibres, particles, or flakes. Generally, materials in the matrix phase are continuous. Composite systems include concrete reinforced with steel and epoxy reinforced with graphite fibres. Normally, two or more constituent materials with considerably diverse physical or chemical properties are joined to generate a material with characteristics that are distinct from the separate components. A nanocomposite is a traditional material that has nanoscale particles or nanostructures scattered throughout the bulk material. Non-nanoscale matrices are commonly used as the basis material. Nanocomposites are often made up of an inorganic (host) solid with an organic component, or two (or more) inorganic/organic phases in some combination. Nanocomposite materials can exhibit a variety of mechanical, electrical,

optical, electrochemical, and other properties. A composite material consists of two phases. In the primary phase, it forms a matrix in which the secondary phase is embedded, which can be polymers, metals, or ceramics. Secondary phase, alternatively referred to as embedded phase or reinforcing agent. It serves to reinforce composites such as fibers and particles and can be one of the three basic components or a chemical element such as carbon or boron. Composites are classified into three categories based on their matrix phase; Metal Matrix Nanocomposites (MMNCs), Ceramic Matrix Nanocomposites (CMNCs), and Polymer Matrix Nanocomposites (PMNCs). Figure 2.1 show illustration of composite matrix and fiber combination.

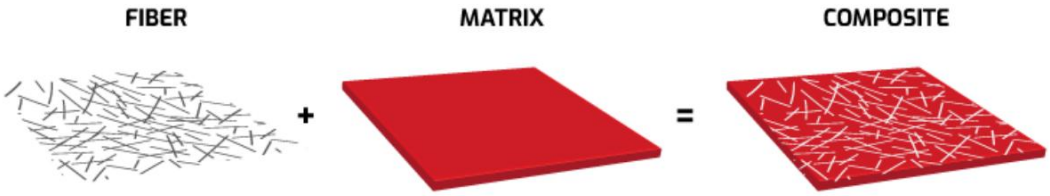

Figure 2.1: The combination of fiber and matrix will produce composite materials. (RomeoRim, 2021).

Each nanocomposite should have two critical dimensions, one upper and one lower. Critical values are determined by the composite's expected property (Kamigaito, 1991). Nanocomposites have the potential to significantly improve mechanical properties such as strength, modulus, and dimensional stability, electrical conductivity, thermal stability, chemical resistance, surface appearance, optical clarity, and gas, water, and hydrocarbon permeability. Nanocomposites are now used in a wide variety of industries, and new applications are constantly being developed. Nanocomposites have a number of applications, including thin-film capacitors for computer chips, solid polymer electrolytes for batteries, automotive engine components and fuel tanks, impellers and blades, oxygen and gas barriers, and food

packaging.

2.3 Polymer Nanocomposite (PNC)

Polymer nanocomposites are materials in which nanoscopic inorganic particles, ranging in size from 10 to 100 Å in at least one dimension, are disseminated in an organic polymer matrix to drastically increase the polymer's performance attributes. Polymer composites are materials in which a polymer is filled with an inorganic synthetic and/or natural compound to enhance one or more properties, such as heat resistance or mechanical strength, or to decrease others, such as electrical conductivity or gas permeability for oxygen or water vapor. Composite materials with complementary properties are used to create composites with tailored characteristics. For instance, when high-modulus but brittle carbon fibers are combined with low-modulus polymers, a stiff, lightweight polymer composite with some toughness is created. Current polymer composites are truly filled polymers due to the lack of strong interaction between the two mixed partners at the interface. Moving from macroscale to micron-scale and even smaller fillers has been a significant advancement in this discipline. Additional materials can be one-, two-, or three-dimensional. In comparison to pure or conventional polymer composites, dispersed nanocomposites exhibit superior properties. Nano additives have a much higher surface area to volume ratio than micro and macro additives. Due to the nanoscale length scale, nanocomposites are typically transparent due to the reduced light scattering.

In recent studies, polymer nanocomposite has been developed with other nano additives such as carbon nanotubes, graphite and other nanoparticles (Mai & Yu, 2007). Since their discovery in 1991, carbon nanotubes have piqued interest due to

their superior elastic modulus, bending strength, aspect ratio, electrical and thermal conductivity, chemical and thermal stability, and absorbability (Mai & Yu, 2007). They could also be used to make microwave absorbers, sensors, and other aircraft components. They consist of two types of polymer composite which are thermoplastic-matrix composites and thermoset-matrix composites. In thermoplastic, the processing of thermoplastics is reversible, and the resin can be shaped into a different shape by simply warming to the procedure temperature. A thermoset matrix is created when a resin system undergoes an irreversible chemical change into an amorphous cross-linked polymer matrix.

2.4 Polyethylene Terephthalate (PET)

Polyethylene terephthalate (occasionally written poly(ethylene terephthalate)), more commonly abbreviated PET is the most widely used thermoplastic polyester resin. (Ji, 2013). It is used in garment fibers, containers for liquids and meals, thermoforming, and engineering resins in combination with glass fiber. PET is a semi-crystalline or amorphous polymer, depending on the processing and heating conditions (Demirel et al., 2011). It may appear transparent (particle size less than 500 nm) or opaque and white (particle size up to a few micrometers) depending on the crystal structure and particle size of the semi-crystalline material. PET is highly flexible material with a stiffness range of semi-rigid to rigid. It possesses superior dimensional stability, impact resistance, moisture resistance, and resistance to alcohols and solvents. Figure 2.2 show the chemical structure of PET which consist of long polymer chain.

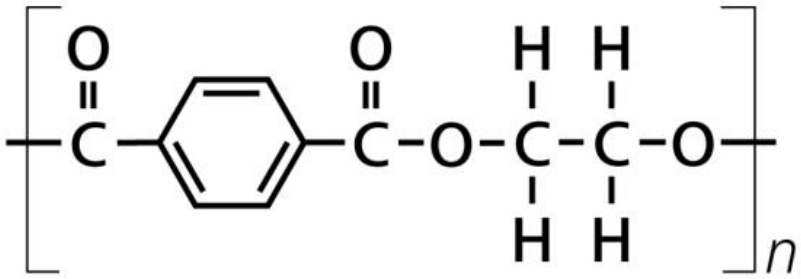

Figure 2.2: The chemical structure of PET chain consists of C, O and H element (Metrohm, 2021).

Numerous advantages of PET have been discovered in recent studies. PET is stronger and stiffer than PBT and has superior insulating properties. When quenched during processing, PET is suitable for transparent applications because it does not break or fracture. It is virtually shatterproof and thus a suitable glass substitute in some applications. PET is already well-known for being a strong and lightweight material that is easy to transport. Besides that, PET has a wider temperature range of use, ranging from -60 to 130°C, and a higher heat distortion temperature (HDT) than PBT. Additionally, PET is well-known for its excellent gas (oxygen, carbon dioxide) and moisture barrier properties, as well as its low gas permeability, particularly when it comes to carbon dioxide. PET is well-known as a recyclable material that is also microwave-transparent. PET is FDA, Health Canada, EFSA, and other health agencies approved as safe for contact with foods and beverages.

PET is combined with other thermoplastics or thermosets to create new materials with improved performance and lower costs to meet the requirements of specific applications. Their thermal, mechanical, impact resistance, and flame retardant properties are significantly improved when thermosets are mixed with PET. These

mixtures are primarily used in the manufacturing of automotive, aerospace, and electrical components.

PET plastic bottles are widely used for mineral water and carbonated soft drinks because polyethylene terephthalate is an excellent water and moisture barrier material (Dupaix, R.B. 2003). Polyethylene Terephthalate films are ideal for use in tape applications due to their high mechanical strength. PET is also used in food packaging, as non-oriented PET sheets can be thermoformed into packaging trays and blisters. It is especially well suited for food packaging applications due to its chemical inertness and other physical properties. Others packaging applications include rigid cosmetic jars, microwavable containers, and transparent films. PET production for synthetic fibers accounts for more than 60 % of global demand, while PET bottle production accounts for approximately 30 % of total demand.

Polyethylene terephthalate is frequently used in the electrical and electronic industries. It is an effective polymer that can be used in place of die cast metals and thermosets in applications such as electrical encapsulation, solenoids, smart meters, photovoltaic components, and solar junction boxes. Polymers' superior flow properties enable design freedom and miniaturization in the manufacture of high-performance products.

PET is a type of polyester that is aliphatic. It is synthesized using polycondensation monomers obtained by esterifying terephthalic acid with ethylene glycol or by trans esterifying ethylene glycol with dimethyl terephthalate. Injection molding (Haddad et al., 2009), extrusion, blow molding (S.H. Masood, 2006), and thermoforming are all simple ways to process PET. PET is typically extruded into films and sheets which can then be thermoformed, whereas transparent bottles are typically blown. It is

strongly recommended that Polyethylene Terephthalate be dried for 2-4 hours at 120 °C prior to processing. It is possible to use up to 25 % regrind.

PET products are 100 % recyclable and are the most recycled plastic on the world. PET is easily identifiable by its recycling code, which is #1. Post-consumer PET bottles are collected and degraded into their raw materials or intermediates, which are then used to create recycled PET flakes through a series of sophisticated washing processes or chemical treatment. Figure 2.3 shows the recycle code of PET that been used world widely. These recycled PET flakes are then used in a variety of applications, including carpet fiber, fleece jackets, comforter fill, and tote bags, as well as food, beverage, and non-food containers, as well as film and sheeting and strapping.

Figure 2.3: Recycle code for PET can identify as recycling code #1 (ism waste & recycling, 2021).

2.5 Carbon Nanotubes (CNTs)

Carbon nanotubes (CNTs) are cylinder-shaped molecules composed of single-layer carbon atom sheets that have been rolled up (graphene). Single-walled carbon nanotubes (SWCNT) have a diameter of less than one nanometer (nm), whereas multi-walled carbon nanotubes (MWCNT) have a diameter greater than 100 nm and are composed of multiple concentrically connected carbon nanotubes. Carbon

nanotubes with a single wall can be visualized as cutouts from a two-dimensional hexagonal lattice of carbon atoms that have been rolled up along one of the hexagonal lattice's Bravais lattice vectors to produce a hollow cylinder. Figure 2.4 shows the structure of SWCNT and MWCNT. Their lengths vary between a few micrometers and millimeters. Carbon nanotubes with a single wall are a carbon allotrope that exists between fullerene cages and flat graphene.

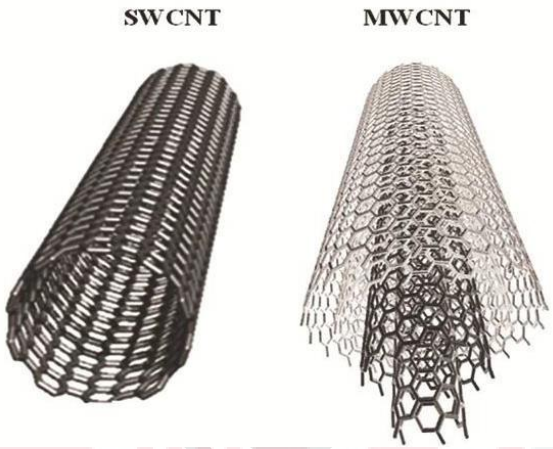

Figure 2.4: Structure of Single-walled Carbon Nanotubes (SWCNT) and Multi-walled Nanotubes (MWCNTs) (Choudhary & Gupt, 2011).

CNTs are chemically bound and extremely strong molecular interactions. This property, combined with the natural tendency of carbon nanotubes to strap together due to van der Waals forces. MWCNTs are tree-ring-like structures composed of nested single-wall carbon nanotubes held together by weak van der Waals interactions. These tubes resemble, but are not identical to, Oberlin, Endo, and Koyama's long straight and parallel carbon layers cylindrically stacked around a hollow tube. Carbon nanotubes with a double or triple wall are also referred to as multi-wall carbon nanotubes.

Chemical bonding in carbon nanotubes enables the development of ultra-strong,

lightweight materials with highly conductive electrical and thermal properties. This makes them extremely versatile for a variety of applications. The electrical properties of nanotubes are determined by the rolling-up direction of the graphene layers, which can be either rolling-up or chiral. The chirality of the hexagonal carbon-atom lattice in the nanotube refers to the angle of the hexagonal carbon-atom lattice in the nanotube.

With the goal of fabricating novel advanced materials with multifunctional capabilities, various approaches for incorporating CNTs in polymer matrices have been developed. Several of these characteristics were developed with the objective of transferring the unique electrical properties of carbon nanotubes to insulating polymer matrices in order to create conducting polymer composites. Due to their extremely high surface-to-volume ratio, geometry, and hollow structure, carbon nanotubes have enormous potential for use in a wide variety of scientific and technological fields, most notably as composite fillers in polymers to improve the mechanical, thermal, and electrical properties of the resulting composites. CNTs have been suggested for use in a variety of applications, including electromagnetic absorption, corrosion protection, reinforced materials in natural fiber composites, electromagnetic interference shielding (EMI), batteries, solar cells, chemical sensors, hydrogen storage, and field-emission materials (Norizan et al., 2020).

In addition to the two basic forms, carbon nanotubes can be classified into three distinct varieties. Carbon nanotubes are classified into three types which are armchair carbon nanotubes, zigzag carbon nanotubes, and chiral carbon nanotubes. The distinction between these two types of carbon nanotubes is the way graphite is "rolled up" during the manufacturing process. SWCNTs can be made in a variety of

configurations depending on the position of the rolling axis in relation to the hexagonal network of the graphene sheet and the radius of the closing cylinder.

The chiral vector is denoted by two integers, m and n, which indicate the number of unit vectors in the grapheme honeycomb crystal lattice in each direction. When m equals 0, the nanotube is called "zigzag," when m equals n, it is called "armchair," and all other configurations are called "chiral."

2.6 Processing and Fabrication of PET-CNTs Nanocomposites

PET/carbon-based composites can be synthesized using conventional mixing techniques, solution blending, melt compounding, or in situ polymerization, which are the most frequently used polymer composite synthesis procedures (Wang et al., 2015). Melt compounding has long been recognized as a simple and efficient method for thermoplastics processing, particularly from an industrial standpoint,among these three processing processes and this approach enables the production of low-cost high-performance thermoplastic nanocomposites, allowing for large-scale commercial applications (Rodríguez-Uicab et al., 2013). Melt blending is a common technique for dispersing carbon nanotubes in a thermoplastic polymer matrix (Alexiou et al., 2020) because it is compatible with modern industrial applications such as extrusion and injection molding (Rane et al., 2018). It disperses nanofillers in a polymer matrix by combining high temperature and strong shear forces, and it is most compatible with present industrial procedures. Melt mixing, on the other hand, is often ineffective at spreading fillers in the PET matrix. Additionally, it is limited to lower concentrations due to the high viscosities of composites with increased nanofiller loadings.

The most challenging aspects of fabricating carbon nanotube/polymer composites are

gaining uniform carbon nanotube dispersion in polymeric matrixes and achieving excellent interfacial interactions between the carbon nanotubes and the matrix (Rodríguez-Uicab et al., 2013). MWCNT/PET composites benefited from in situ polycondensation in terms of tensile strength and elastic modulus (Zhu et al., 2011), and it was found that melt copounding PET/MWCNT composites in a twin-screw extruder improved their mechanical properties, which also was contributed to the good dispersion of MWCNTs in the PET matrix (Kim et al., 2007). MWCNTs were dispersed in PET without using solvents and then melt blended, resulting in MWCNT/PET composites with superior mechanical properties and a higher crystallization temperature. (Santoro et al., 2010). The polymer processing method has an effect on the mechanical and electrical properties ofcomposites, and the most common methods include melt compounding, extrusion, and/or dissolution (Rodríguez-Uicab et al., 2013).

2.7 Electromagnetic Shielding

Electromagnetic (EM) shielding is a conductive or magnetic electromagnetic shell that forms a tight electromagnetic shielding region and shields the electromagnetic wave. EMI shielding is the process of shielding radio frequency or microwave radiation in a shield that acts as a radiation barrier (Chung, 2020). Through reflection, absorption, and attenuation, shielding materials are used to limit the electromagnetic field effects of radiation sources. When an electromagnetic signal reaches the surface of shield materials, it is reflected, absorbed, and refracted (Triantafillou, T, 2017).

Shielding can be used to reduce radio waves, electromagnetic fields, and electrostatic fields. Faraday cages are conductive enclosures used to protect against electrostatic

fields. The magnitude of the reduction is highly dependent on the material used, its thickness, the size of the shielded volume, the frequency of the fields of interest, and the size, shape, and orientation of holes in a shield with respect to an incident electromagnetic field. Furthermore, depending on the frequency, electromagnetic waves can not only travel in a straight line but can also be diffracted like light. As a result, while utilizing a shielding material, keep in mind that the electromagnetic wave may diffract around the shield and reach the shielded area.

Electromagnetic waves can be attenuated by reflecting or absorbing received energy (Marra et al., 2018). Reflection loss happens at the point when the shielding material meets the air. Regardless of the shield thickness, the conductivity of the shielding material determines the level of loss. The surplus current generated when the electromagnetic wave travels through the shielding material causes absorption loss. The shielding material's thickness, magnetic permeability, and conductivity all have an effect on the level of loss. Multiple reflections of the electromagnetic wave occur within the shielding material, resulting in multiple reflection loss (Kolanowska et al., 2018).

2.8 Electromagnetic Wave Shielding Application

Electric and magnetic fields are connected in electromagnetic radiation. The charge carriers in the conductor are subjected to forces created by the electric field. When an electric field is applied to the surface of an ideal conductor, it induces a current that results in charge displacement within the conductor, cancelling the applied field and bringing the current to a stop. Eddy currents are generated when magnetic fields change, and they cancel out the applied magnetic field. As a result, electromagnetic radiation is reflected from the conductor's surface, with internal fields remaining

within and exterior fields remaining outside. Radios, antennas, cell phones, the Global Positioning System (GPS), Bluetooth (a wireless standard for exchanging data between mobile and fixed devices over short distances), Wi-Fi, and microwave devices are all radio wave or microwave radiation dependent. Antennas, which operate in the radio wave and microwave regimes, can benefit from highly conductive materials that are common in EMI shielding materials (Chung, 2020). Wireless communication is required for Internet of Things (IoT) devices, radio frequency identification device (RFID) tags, autonomous vehicles, wearable (stretchable) electronics, and virtual/augmented reality (Chung, 2020).

Radio waves cannot be reflected by ordinary concrete. A conductive component such as carbon fiber can be added to concrete to impart this property. This capability is advantageous for vehicle lateral guidance on automatic highways (Chung, 2020).

2.9 Electromagnetic Mechanisms

Reflection, absorption, and multiple reflection are three mechanisms that have been claimed to be involved in EMI shielding as shown in Figunre 2.5. Reflection is often the principal shielding mechanism for a sheet of homogeneous conductive material which not a mixture of aconductive filler and an insulative matrix. The material must contain mobile charge carriers (electrons or holes) that interact with the incoming electromagnetic waves to provide reflection protection (Sotiropoulos et al., 2021).

The second major mechanism is absorption, which is dependent on the shield thickness. When the shielding material has electrical or magnetic dipoles that interact with the EM waves,absorption shielding is improved. The third shielding mechanism is multiple reflection, which represents internal reflections within the shielding

material (Chen.et.al., 2010). Multiple reflection reduces total shielding when the shield is thinner than the skin depth, and if the shield is thicker than the skin depth, it can be ignored (Sotiropoulos et al., 2021). The strength of an electromagnetic wave decreases dramatically as it travels through a conductive medium (Karimi et al., 2016).

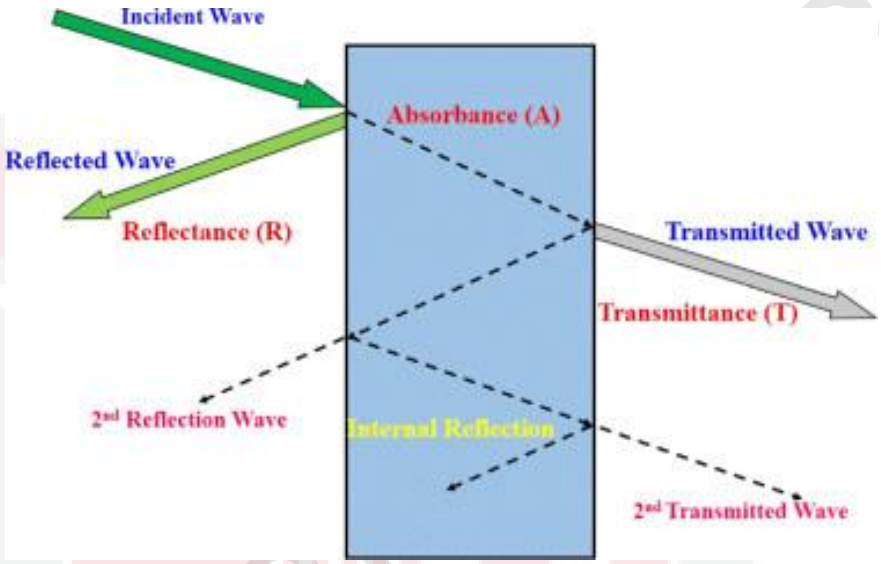

Figure 2.5: There are three behaviors of electromagnetic mechanism (Joshi & Datar, 2015).

2.9.1 Reflection

The shield must contain mobile charge carriers such as electrons or holes that interact with the electromagnetic fields in the radiation to reflect the radiation. As a result, even when a high conductivity is not required (Jaroszewski et al., 2019), the shield tends to be electrically conducting (Vargas-Bernal, 2015). Electrical conductivity is not a scientific requirement for shielding, as conduction requires connectivity in the conductor, whereas shielding does not. While shielding is not required for connectivity, it benefits from it.

2.9.2 Absorption

Receipt of electromagnetic radiation by charged particles, resulting in the transfer of the radiation's energy and momentum. Electromagnetic waves, photons, and light are all terms used to describe electromagnetic radiation. Any particle with an electric charge can absorb electromagnetic radiation. Photons are fundamental particles that carry electromagnetic energy and manifest as light with a range of energies or wavelengths. Any charged particle, such as an electron, can absorb light. The absorbed light is annihilated in the sense that its energy and momentum are transferred to the charged particle, leaving no individual photons of light. The apparent appearance of objects is determined by the absorption of the absorbed energy can be used to increase the kinetic energy, potential energy, or the energies of both charged particles, resulting in heating and atomic transitions. Ionization and radiation pressure can occur because of the absorbed momentum changing the particle's velocity. The absorption of electromagnetic radiation causes heating, ionization, fluorescence, and other consequences.

2.9.3 Multiple Reflection

Multiple reflections refer to the reflections at various surfaces or interfaces within the shield. This mechanism requires a large surface area or interface area in the shield. A shield with a large interface area is exemplified by a composite material containing a large surface area filler. When the distance between the reflecting surface faces or interfaces is large in comparison to the depth of the skin, the loss caused by multiple reflections can be ignored.

2.10 Characterization

The phase, structure, morphology, and wave absorption impacts of the samples are determined using a few characterization methods in this study. Characterization is necessary since the research findings can be compared to the existing theory. X-Ray Diffraction (XRD), Field Emission Scanning Electron Microscope (FESEM), Vector Network Analyzer (VNA) and Two-point Probe were used to characterize the samples in this investigation.

2.10.1 X-Ray Diffraction

X-ray diffraction analysis (XRD) is a technique used in materials science for determining the crystallographic structure of a material. XRD is a technique that involves irradiating a substance with incoming x-rays and then measuring the intensities and scattering angles of the resulting x-rays. XRD analysis is frequently used to identify materials based on their diffraction pattern. Additionally, to phase identification, XRD provides information on how the actual structure differs from the ideal structure due to internal tensions and flaws.

X-rays are electromagnetic waves, whereas crystals are ordered arrangements of atoms. Scattering of incident x-rays occurs as a result of the interaction of incident x-rays with the electrons of crystal atoms. Figure 2.6 illustrate the mechanism of x-ray diffraction. This phenomenon is referred to as elastic scattering, and the electron is the scatterer. A regular array of scatterers produces a regular array of spherical waves. Due to destructive interference, these waves cancel out in the majority of directions, but add constructively in a few select directions, as indicated by Bragg's law:

$$2\,d\,\sin\theta = n\,\lambda \qquad (1)$$

Where d denotes the distance between diffracting planes, θ denotes the incidence angle, and n denotes an integer. The diffraction pattern reflects the specific directions. X-ray diffraction patterns are formed when electromagnetic waves impinge on a regular array of scatterers. Since their wavelength, λ is frequently the same order of magnitude as the distance, *d*, between the crystal surfaces, x-rays are used to create the diffraction pattern (1-100 Å).

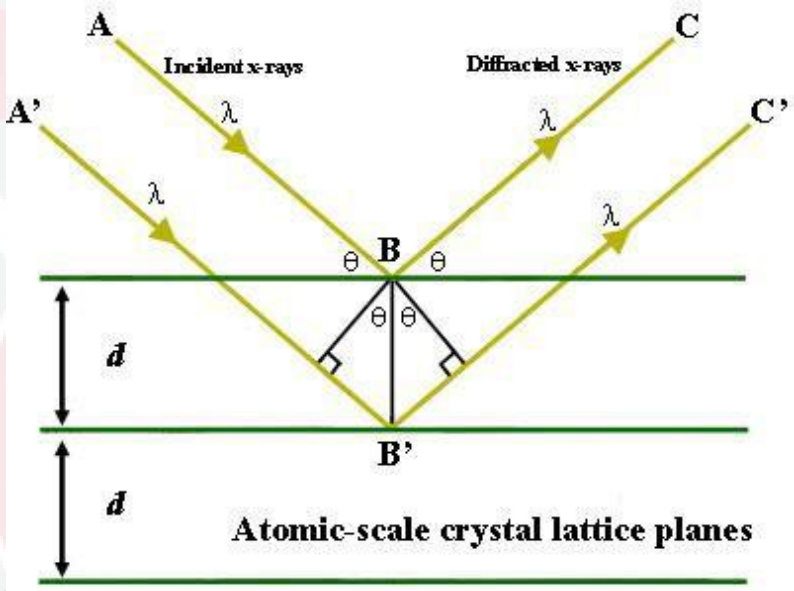

Figure 2.6: Bragg's Law reflect X-ray beams at specific incidence angles (Henry et al., 2016).

XRD is a non-destructive technique for determining structural features such as lattice parameters, strain, and grain size, as well as identifying crystalline phases and orientation. It is useful for determining the thickness of thin films and multilayers, as well as determine the atomic arrangement, using epitaxy. phase composition and preferred orientation.

2.10.2 Field Emission Scanning Electron Microscope (FESEM)

FESEM is an abbreviation for Field Emission Scanning Electron Microscope. A FESEM is a microscope that operates on the principle of electrons (negatively charged particles) rather than light. These electrons are liberated by a field emission source. Electrons are used to scan the object in a zig-zag pattern. It is a device that allows for the visualization of extremely fine topographic features on the surface of whole or fractionated objects. Biologists, chemists, and physicists use this technique to detect structures as small as 1 nanometer. The FESEM is useful for studying organelles and DNA material within cells, as well as synthetic polymers and microchip coatings. A Jeol 6330 microscope, coupled with a specific freeze-fracturing apparatus, has been used as an example for the virtual FESEM (Oxford Ato).

Figure 2.7: Field Emission Scanning Electron Microscopy Machine for determination of surface morphology (UPM, 2020).

FESEM as shown in Figure 2.7 operates by accelerating electrons in a strong electrical field gradient following their liberation from a field emission source. Electronic lenses within the high vacuum column focus and deflect these so-called primary electrons to create a narrow scan beam that bombards the item. As a result, each spot on the object emits secondary electrons. The angle and velocity of these secondary electrons are dependent on the surface structure of the object. A detector detects the secondary electrons and generates an electronic signal. This signal is amplified and converted toa video scan image that can be viewed on a monitor or saved and further processedas a digital image.

2.10.3 Vector Network Analyzer (VNA)

A Vector Network Analyzer (VNA) is a resistance meter similar to a multimeter. Unlike a multimeter, which measures a resistor at DC (0 Hz), a VNA detects the resistance of an RF or microwave circuit at its operating frequency, capturing both the resistance and phase of the circuit, which together form a Vector. Additionally, a VNA can determine the magnitude and phase of the gain or loss between two circuit ports. Additionally, by measuring a range of frequencies, they generate a graph of impedance and gain over that frequency range. Figure 2.8 show VNA machine model that used specially to analyze EMI shielding.

To make RF and microwave devices function together efficiently, a VNA is utilized to characterize them. The output impedance of one component must match the input impedance of the next component for the RF system to work properly. Antennas come in a wide variety of impedances, which must be determined and matched to the devices they connect.

Figure 2.8: Vector Network Analyzer (VNA) Machine to observe the EMI absorbance properties (UPM, 2021).

When a known signal source is connected to the device being tested, the VNA measures the voltage across the device's terminals, which are typically the signal and ground of a coax connection. It can calculate the complex impedance based on the known source and the measured signal. The VNA, on the other hand, contains a built-in RF signal generator to measure at RF frequencies, whereas a multimeter needs DC from a battery and the measuring circuit compares the amplitude and phase of the measured signal to those of the source. The VNA supplies the same source signal to one port and measures the output signal from the device under test's other port to determine gain or loss.

2.10.4 Two-Point Probe

The two-point probe technique is ideal for determining the resistivity of high-resistance material, such as polymer films and sheets. The two-point or resistance measurement technique involves passing an electrical current between two probes separated by a few millimeters and measuring the potential difference between them

(Lataste, 2010). The resistivity is computed as follows using the voltage drop, V and current, I.

$$\rho = \frac{A}{IL} \tag{2}$$

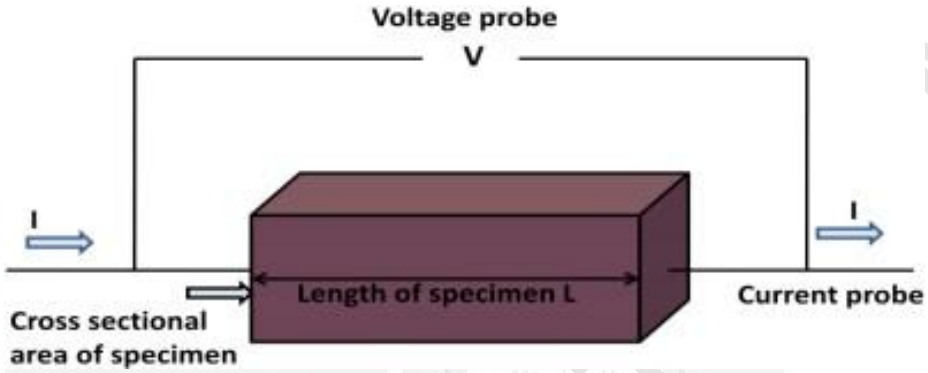

Figure 2.9: The behaviour of two-point probe technique to measure electrical conductivity.

In this study, we focus on the conductivity of the sample. Using this method, the conductivity can be calculated since

$$C = \frac{1}{\rho} \tag{3}$$

The bulk electrical conductivity of the samples was calculated using this formula:

$$\sigma = \frac{I}{V} \cdot \frac{L}{w \cdot t} \tag{4}$$

where;

L = the length of the measured segment

w = the width

t = the thickness

V/I indicate the conductance, C

CHAPTER 3: METHODOLOGY

3.1 Raw Materials

This experiment required two main materials, namely Poly(ethylene Terephthalate), PET and Carbon Nanotube, CNTs. G084A type thermoplastic PET used as matrix fabrication in PNC. It was purchased with 100 % purity from Recron Nilai Bhd. Figure 3.1 show the raw PET sample. The CNTs (773840) contained ≥ 98 % carbon with a diameter of 10 nm and a length of 3 ~ 6 μm. Any raw materials used of carbon in this study are without modification or refinement.

Figure 3.1: The PET sample with 100 % purity used.

3.2 Preparation of Materials

In this study, there are two compositions of the nanofillers that were synthesized: 0.1 wt.% and 0.5 wt.% nanofillers. Pure PET, PET-CNTs with 0.1 wt.% and 0.5 wt.% were produced. All samples were prepared according to the composition percentage as stated in Table 3.1. There were three key stages required in the preparation and production of these samples involved drying weighing, melt blending and injection molding as shown in Figure 3.2. Then, some of the sample was ground to meet the requirement for the characterization method: such as for Vector Network Analysis (VNA) and Two Point Probe.

Table 3.1: The samples were prepared according to these weight percent to fabricate PET nanocomposite.

Sample	PET (wt.%)	CNTs (wt.%)
PET	100.0	0.00
PET/CNTs 0.1 wt%	99.9	0.10
PET/CNTs 0.5 wt %	99.5	0.50

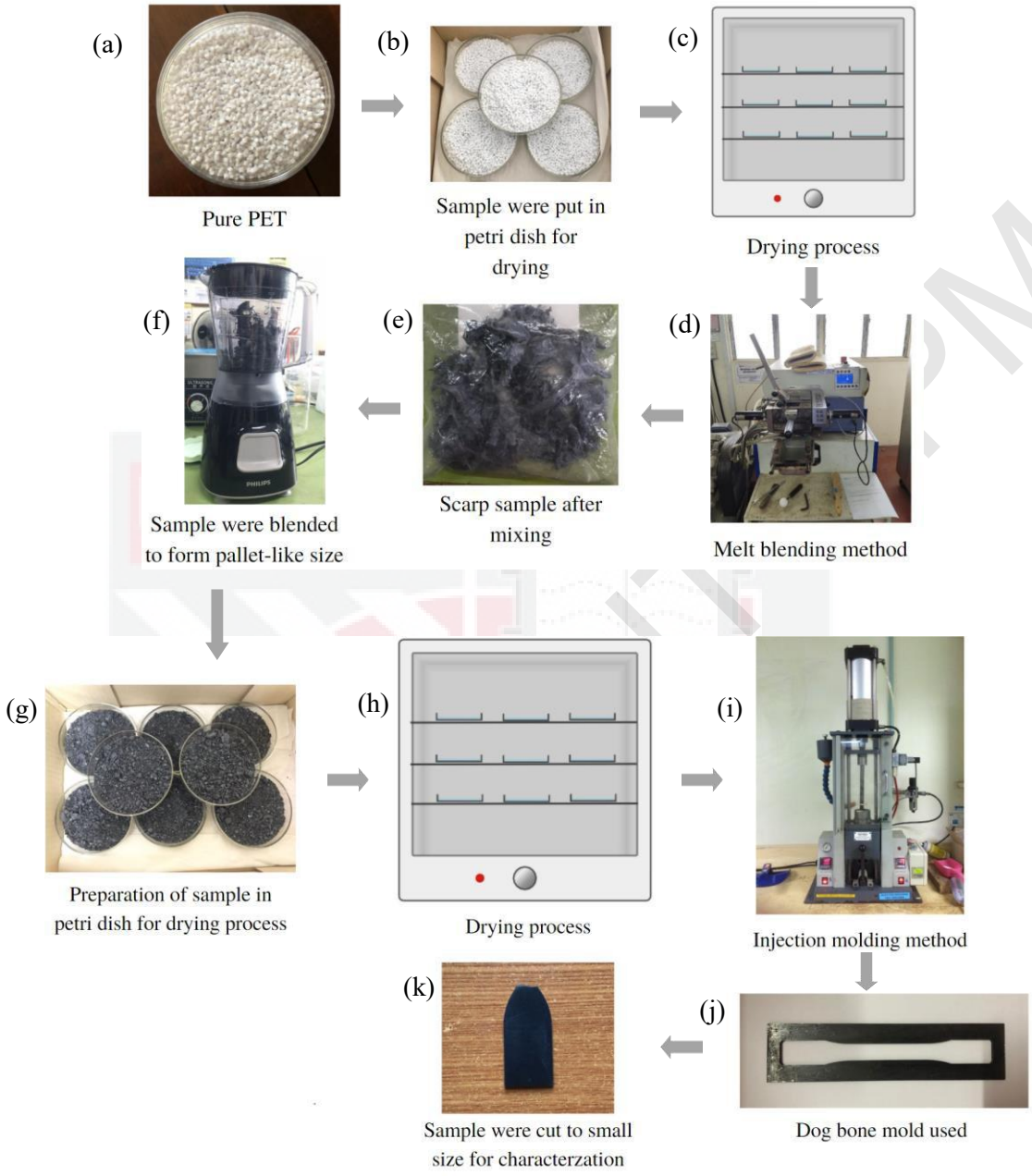

Figure 3.2: Schematic representation of PET-CNTs sample preparation and characterization in this study (a - k)..

3.2.1 Drying and Weighing

All of the materials were dried to remove excess moisture. Moisture in the filler can produce defects in the produced nanocomposites, such as voids and pinholes. The samples were placed in a petri dish and dried for 24 hours at 120 °C in an oven. Following the drying process, the samples were weighed using the HAAKE blending machine's test weight formula. Then it was labelled and stored in the presence of a humidity absorbent for storage. Figure 3.3 illustrate the preparation for dying process. Equation (5) used for calculating the ration of theraw sample to produce the exact weight percent nanofiller required using HAAKE blending machine to fabricate PET nanocomposite.

$$\mathrm{m} = \rho \times Vn \times t \times wt\% \qquad (5)$$

Since,

m = the test weight,

t = the filling rate,

ρ = density of the material,

V_n = net volume

wt.% = the weight percentage of each material in the mixture,

Figure 3.3: The PET sample were divided to several parts inside the petri dish for drying process.

3.2.2 Melt Compounding

The most suitable method for fabricate polymer nanocomposites of a thermoplastic's matrix is melt blending (Rane et al., 2018). Melt-blended PET-CNTs were formed by melt compounding mixtures of a PET and different percent of CNTs which were 0.1 wt.% and 0.5 wt.%. Compounding was done for 10 minutes on a HAKKE melt-blending machine at the Institute of Tropical Forestry and Forest Product (INTROP) in UPM as shown in Figure 3.4. The weighed samples were placed in the mixing partition. The machine was put together with PolyLab Monitor software and the temperature for processing was set to 250 °C with a 500 rpm rotating speed. Compositions containing 0.1 wt.% and 0.5 wt.% were mixed and solidified in the air until the ambient temperature was obtained. PET without addition of filler also prepared in this study.

Figure 3.4: HAAKE Melt Blending machine used to mixing the PET and CNTs for fabrication of PET nanocomposite.

3.2.3 Injection molding

The hardened samples were crushed with a home blender using PHILIPS HR2506 Blender to produce small size, it is because the mold only accepts a pellet-like size sample to ease the casting process. Then, all the nanocomposite pellets were dried again using temperature of 100 °C for 12 hours to remove the moisture and form injection molding using Ray Ran Injection Molding machine at INTROP in UPM to fabricate the sample. Figure 3.5 show the injection molding press that used in this method. The hardened samples were then put into the injection molding machine. The temperature of the barrel and mold were set to 280 °C and 30 °C, respectively. Approximately 10 grams of the crushed sample are put in the barrel for 6 minutes to melt before the injection process is carried out using the provided machine. The injection time was set to 6 seconds at a pressure of 7 bar. After a couples of minutes,

the air pocket was removed, and the mold was inserted using mold size in Figure 3.6.

Figure 3.5: The injection molding method were conducted using Ray Ran Injection Molding Press.

Figure 3.6: All the sample are casting using dog bone mold.

3.3 Characterization

X-Ray Diffraction (XRD), Field Emission Scanning Electron Microscope (FESEM), Vector Network Analyzer (VNA), and Two-point probe were used as characterization methods in this study. The next sections go into the specifics of each characterization approach used.

3.3.1 X-Ray Diffraction

After the sample was cut into the appropriate size for the x-ray diffraction characterization as shown in Figure 3.7, and all samples' crystal structure and crystallinity were evaluated. The specimens' x- ray diffraction patterns were obtained in reflection mode using a PANalytical PRO PW3040 x-ray diffractometer at the Faculty of Science, UPM as shown in Figure 3.8. Copper anode CuK (wavelength = 1.5406) radiation was used for the x-ray beam. The diffractometer was run at a current of 40 mA and an accelerating voltage of 40 kV. The 2θ from 20°to 80° range was scanned at a rate of 0.1°/min. The data was then examined with the X'pert HighScore programme. The overall crystalline fraction was calculated using this approach, as well as the parameters for each crystal peak.

(a) PET (b) PET-CNTs 0.1 wt.%

(c) PET-CNTs 0.5 wt.%

Figure 3.7(a)(b)(c): The molded samples were cut to small size for undergo characterization.

Figure 3.8: XRD instrument model PANalytical PRO PW3040 that been use in this study.

3.3.2 Field Emission Scanning Electron Microscopy (FESEM)

The small sample size was required to analyze the dispersion of the nanocomposite polymer matrix as shown in Figure 3.7. The tested samples were coated with Au / Pd prior to the measurements. The FESEM was used to examine microscopy in the Institution of Advance Technology (ITMA), Faculty of Engineering, UPM as shown in Figure 3.9. The tested samples were coated with Au/Pd prior to the measurements. It is to make a non-conductive material become a conductive material. Data was collected at magnifications of 5k, 10k, 25k, and 50k.

Figure 3.9: FESEM instrument model that been used in this study (ITMA, 2021).

3.3.3 Vector Network Analysis (VNA)

The sample were cut to small pieces and were grinded using sandpaper to get the required thickness for run this characterization as shown in Figure 3.11. The sample also were polish using sandpaper to get the smooth surface to avoid air gap. All sample has constant thickness value which is 1.60 mm that were measured using

electronic digital caliper.The S parameter for the composite sample was measured at room temperature using a Vector Network Analyzer (N55227A) as shown in Figure 3.10 in the frequency range of 8-18 GHz. Before calibrating the analyzer for reflection and transmission, the test normalization procedure was carried out. Polymer nanocomposite samples are measured with the same conditions, including power level and measurement frequency. The air gap was closed during the analysis to prevent interference when measuring transmission, reflectivity, and absorption. From the measured S-parameter values, the sample's real and imagined permeability and permeability values are derived. Equation (6) were used to determine the total shielding effectiveness, SE_T while Equation (7) and (8) used to calculate the absorption effectiveness and reflection effectiveness respectively of all samples.

$$SE_T = SE_A + SE_R = 10 \log \left(\frac{1}{|S_{21}|^2}\right) \quad (6)$$

$$SE_A = 10 \log \left(\frac{1-|S_{11}|^2}{|S_{21}|^2}\right) \quad (7)$$

$$SE_R = 10 \log \left(\frac{1}{1-|S_{11}|^2}\right) \quad (8)$$

Figure 3.10: The VNA machine model used to determine the shielding effectiveness, SE.

(a) PET (b) PET-CNTs 0.1 wt% (c) PET-CNTs 0.5 wt%

Figure 3.11: Samples were grinded using sandpaper to get required thickness.

3.3.4 Two Point Probe

KEITHLEY 236 Source Measure Unit as in Figure 3.12 were used to measure the conductivity of the materials by using two-point probe configuration. The purpose of this measurement is to determine conductivity of the sample with different composition of nanofiller. Conductivity is an important parameter which can be dependent to the EMI absorbance. This configuration consists of two terminal which will arrange at both side of the sample to measure the bulk conductivity of the sample. The applied voltage goes through to the probe and then the difference in current will be measured by the other probe. The voltage used in this study were set from -100V to 100V. The conductivity can be calculated by this process. The sample used same as used in VNA characterization that shown in Figure 3.11.

Figure 3.12: The electrical conductivity was conducted using two-point probe method (UPM, 2021).

From the raw data, the conductance and resistance value were determined, and the conductivity of the sample can be calculated by using Equation (4). To avoid inaccurate results later, make sure there is no air gap between the tips and sample surface. The table used for measured should not be the conductive materials to avoid current flow.

CHAPTER 4: RESULT AND DISCUSSION

4.1 Introduction

This chapter discusses the outcomes of numerous analyses and characterizations carried out during the research period. This chapter will cover the phase analysis, morphology analysis, and structure of PET-CNTs nanocomposites with 0.1 wt% and 0.5 wt% carbon nanofiller compositions. The characterization method of X-ray Diffraction (XRD), Field Emission Scanning Electron Microscope (FESEM), Vector Network Analysis (VNA), and Two-point Probe were applied in this study. Many interesting and useful results are successfully obtained in parallel with the expected result in this research, which will be detailed in the next section.

4.2 Phase Analysis

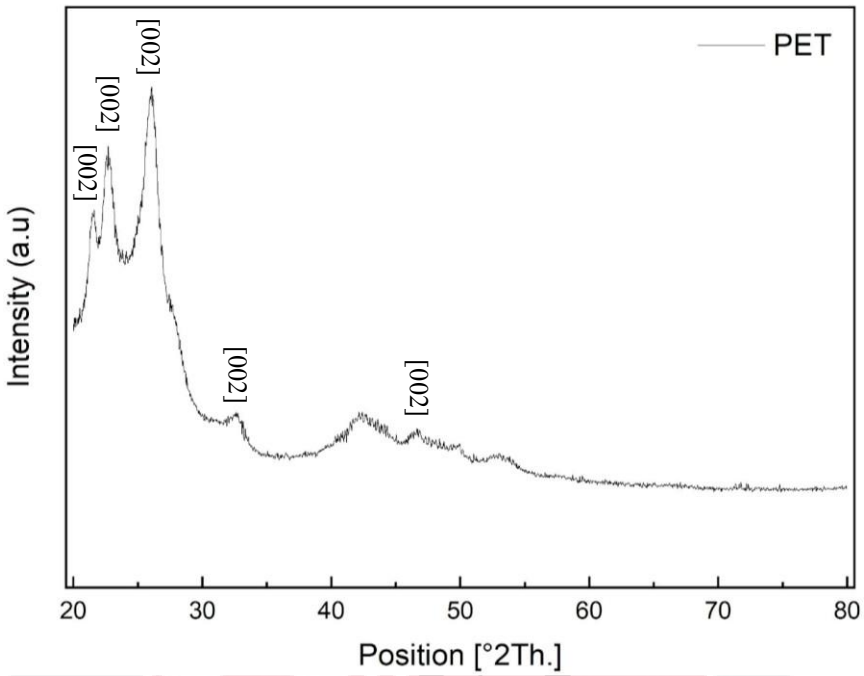

Figure 4.1: XRD profile of pure PET.

X- ray diffraction analysis was conducted to observe the development of the semi-crystalline phase in all the samples. Figure 4.1 illustrates the XRD pattern of pure PET without fillers. Based on the investigation, pure PET has a semi-crystalline structure with crystalline and amorphous areas, with the highest peak at 2θ= 26.1 °. More specifically, the peaks corresponding to crystalline PET at 21.4 °, 22.8 °, 26.1 °, 27.8 °, 32.7 ° and 46.7 ° are detectable. The lattice parameter for PET 100% is a = b = 2.4700 and c = 6.7900. Pure PET having a phase at (0 0 2) phase with hexagonal crystal structure. Using X-pert HighScore, the crystallite size of the PET sample was calculated and given a value of 31 Å.

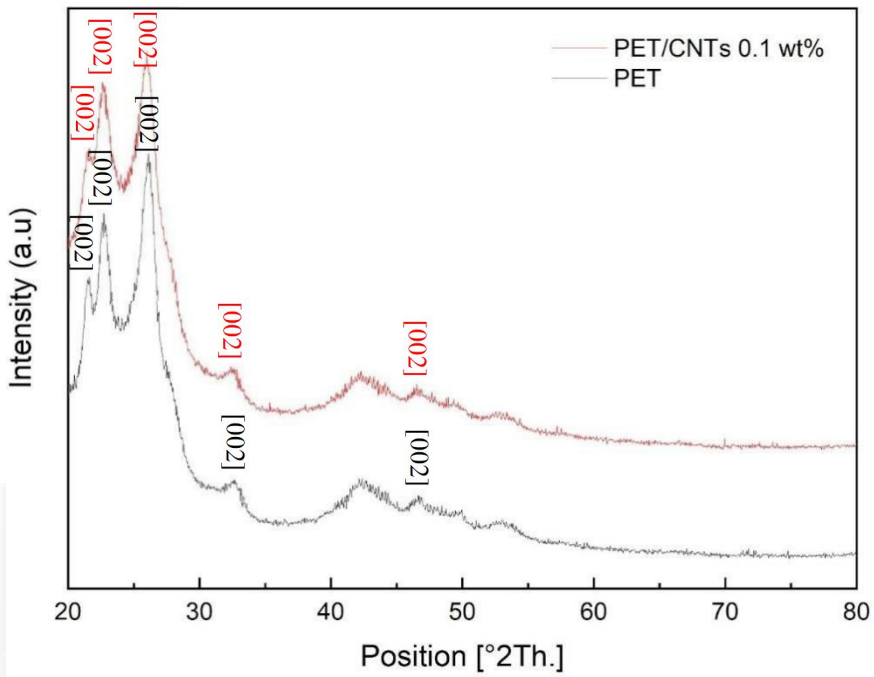

Figure 4.2: Comparison of neat PET with the PET-CNTs 0.1wt.% nano-filler.

The XRD pattern of PET with 0.1wt% carbon nanotubes fillers is shown in Figure 4.2. PET-CNTs 0.1wt.% has the same crystalline pattern which is a semi-crystalline pattern with crystalline and amorphous phase. According to the figure, the peak list for this sample is 21.5 °, 22.7 °, 26.0 °, 32.6 ° and 46.5 ° with the highest peak at 2θ= 26.0 °. PET with nano-filler 0.1wt.% of CNTs has the same lattice parameters with pure PET, which is a = b = 2.4700 and c = 6.7900. This sample also has the same crystal structure and plane phase (0 0 2) with a hexagonal crystal structure. The crystallite size value was calculated using the Scherrer equation given a value of 31 Å.

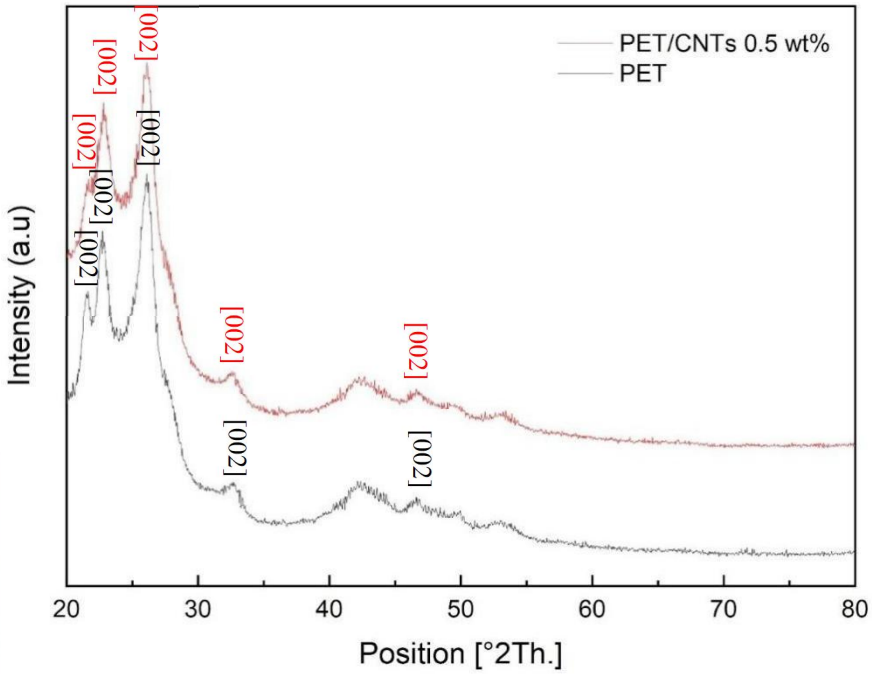

Figure 4.3 PET-CNTs nanocomposite with 0.5 wt.% and pure PET peak pattern.

Figure 4.3 depicts the XRD pattern of PET-CNTs 0.5wt.%. PET with 0.5wt.% CNTs nano-filler has a semi-crystalline peak pattern with crystalline and amorphous phases. The peak list for this sample is 21.5 °, 22.8 °, 26.2 °, 27.8 °, 32.6 °, 46.7 °, and 53.2 °, with the highest peak at 2θ= 26.2 °, as shown in figure above. PET with 0.5wt.% of CNT nanocomposite has the same lattice parameter as pure PET and PET/CNTs with 0.1wt.% which is a = b = 2.4700 and c = 6.7900. PET/CNTs 0.5wt.% has the same crystal structure as the lower nano-filler nanocomposite, with a hexagonal crystal structure and the (0 0 2) plane phase. The crystallite size for PET-CNTs 0.5wt.% nanocomposite is 31 Å.

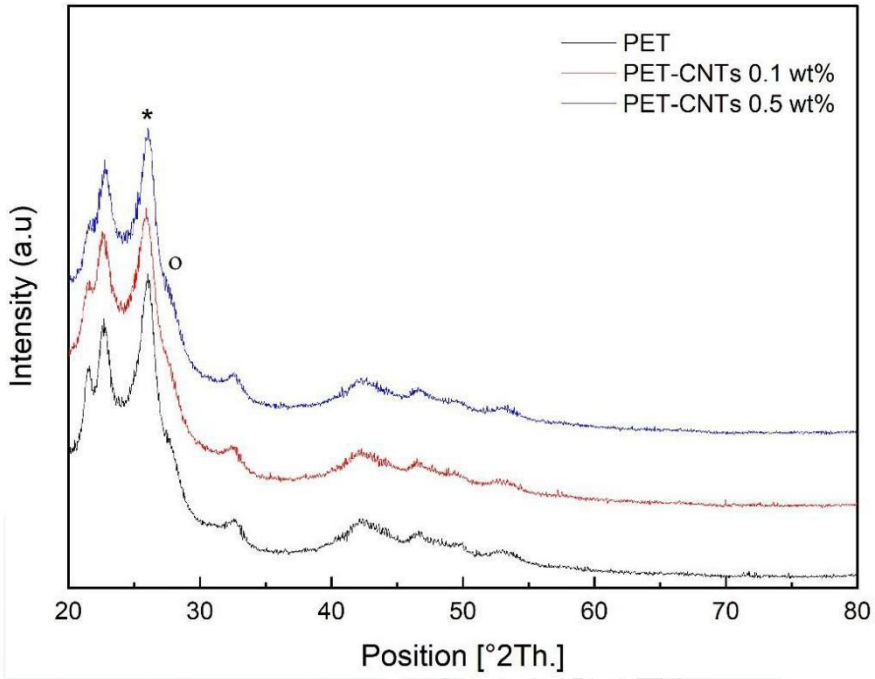

Figure 4.4 Comparison of the peak pattern for neat PET, PET-CNTs 0.1wt.% and PET-CNTs 0.5wt.%.

According to the data above, all the samples had a semi-crystalline XRD pattern with a slightly different peak. Figure 4.4 illustrates the XRD patterns of pure PET and PET nanocomposites with different CNTs nano-filler range of 0.1 and 0.5wt.%. The diffraction peaks of PET-MWCNT nanocomposite for 0.1wt.% and 0.5wt.% are at 2θ = 26.0 ° and 2θ = 26.2 °. For neat PET, the semi-crystalline diffraction peak was seen to have a similar peak high with the PET nanocomposite. However, the PET nanocomposites 0.5wt.% have slightly higher peaks compared to PET-CNTs 0.1wt.% followed by neat PET. Hence, the specific high of XRD peaks were even marginally detectable for samples loaded with CNTs. The following diffraction peaks at 2θ degrees have been ascribed to crystal faces for highly crystalline PET: (002) = 25.5 °, (001) = 41.6 °, (011) = 43.7 °, (012) = 49.5 °, (004) = 52.6 °, and (013) = 58.3 ° [22,38,39]. All these samples have the same phase which is (0 0 2) phase, with hexagonal crystal structure. Furthermore, the crystallite size for PET is 31 Å

while the PET with 0.1 and 0.5wt.% nano-filler also share the same crystallite size value. Moreover, the peak size of PET is broad compared to PET-CNTs nanocomposite 0.1wt.% and narrower for CNTs nano-filler 0.5wt.%. Based on previous study, the peak size is inversely proportional to the crystallite size as the peak narrower, the crystallite size will increase. But in this case, the crystallite size shares the same value for all samples as the highest peak size did not show a significant difference.

The nucleating effect of CNTs has promoted the PET crystallization and similar diffraction peaks are observed when MWCNT fillers loading increases (Alexiou et al., 2020) as the rate of crystallization is accelerated by the nucleating effect (Wypych, 2016). In contrast, the peak slightly increases and narrower as the CNTs tend to improve the crystallization but PET peaks overshadow the CNTs peak and illustrate in minor different of the peak. Hence, from the observation from Figure 4.4, the slightly increasing peak characteristics can be observed where the PET-CNTs nanocomposite have narrower peaks than PET which have a broader peak. Thus, the higher weight percent of CNTs loaded, the higher and narrower the peak. It is because the CNTs have crystalline properties and it tends to influence the neat PET peaks which have amorphous properties. For example, this situation can be analyses around at $2\theta=28°$ indicating by O in Figure 4.4, there is a slightly increasing in peak pattern at PET-CNTs 0.5wt.% compared to 0.1wt.% and pure PET that more board, when the amounts of nano-filler is increase, the crystallinity of the PET nanocomposite improved. The nucleating agents can significantly increase the density of nuclei, thereby increasing the crystallization temperature, increasing the rate of crystallization, and decreasing the spherulite size. Clearly, the existence of CNTs improves crystallinity due to their nucleating effect.

In all PET-CNTs compositions, the latter peak is overshadowed by the PET peak as the PET peak is higher and broader than CNTs. The addition of CNTs did not alter much for the peak pattern and position of PET nanocomposites, indicating that the polymer nanocomposites retained their phase structure (Alexiou et al., 2020).

4.3 Morphology Structure Analysis

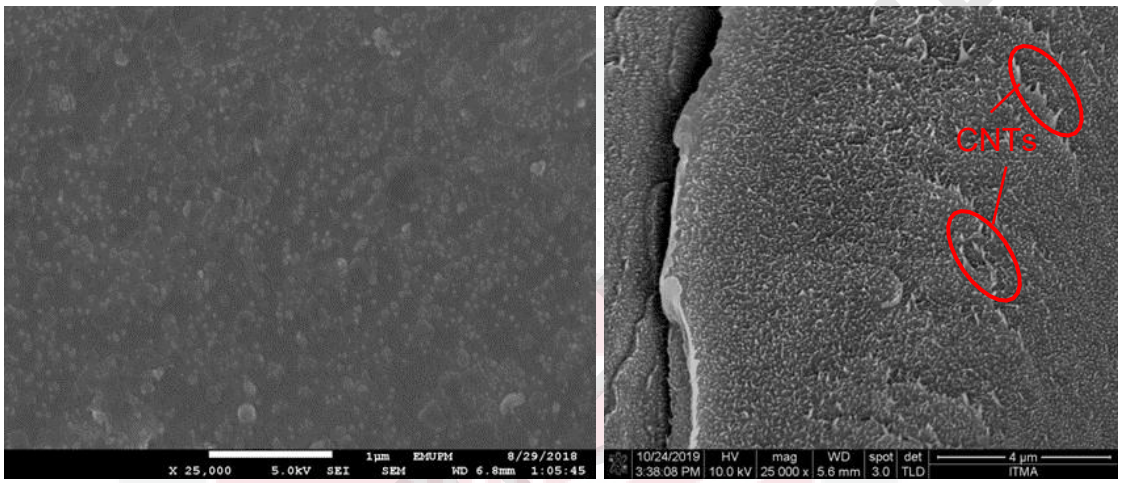

(a) 2(b)

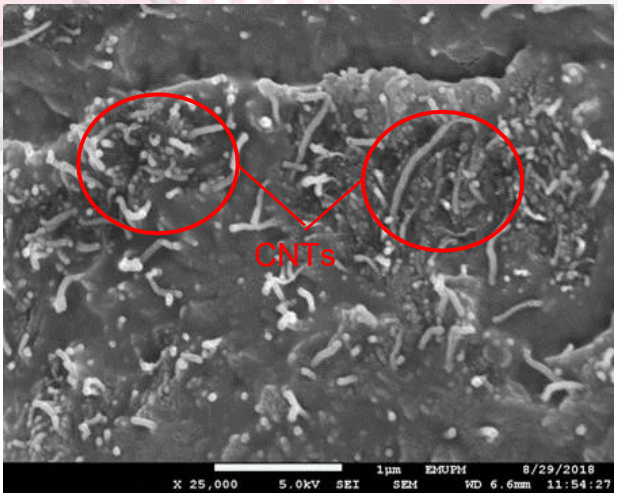

(c)

Figure 4.5(a)(b)(c) Morphology structure of all the sample.

Figure 4.5 shows the image of the fracture surface area of PET without filler, PET-CNTs 0.1wt.% and PET with 0.5wt.% CNT filler that were collected at 25 k magnifications to explore the blend morphology and CNTs localization. Figure 4.5(a) indicates smooth surface structure of pure PET and white patches has been seen in the sample as it is absent in carbon fillers. The fractured surface of pure PET was flat, and it showed a homogeneous continuous phase.

Furthermore, the morphology structure of PET/CNTs with 0.1wt.% filler in Figure 4.5(b) shows rough texture and the filler particles unevenly disperse with the existence of the thread-like structure protruding out from the sample. But it can be considered to have better dispersion and homogenous structure since the filler is well distributed. The FESEM images of the fracture surface area of PET/CNTs 0.5wt.% illustrate the rougher texture with slightly uneven dispersion of the fillers and the thread-like structure appears clearly to be protruding out from the sample. In addition, the bright spots in the images appear to be CNTs, whereas the black backdrop is the PET matrix, based on a comparative examination of samples without CNTs and samples with CNTs integration.

In the pure PET, the fracture structure is smooth compared to PET/CNTs 0.1wt.% and PET/CNTs 0.5wt.% as pure PET does not consist of any fillers. The morphology surface of PET/CNTs 0.5wt.% filler is rougher than PET/CNTs 0.1wt.% as it contains more fillers and the thread-like structure clearly to be seen in 0.5wt.% compared to 0.1wt.%. In the PET FESEM image, they are absent in white patches because the pure PET sample could not fully disperse during processing. The melting parameter of melt compounding is higher than the melting point of PET, which necessitates this patch. As a result, the dispersion was not evenly distributed (Wypych, 2016).

The image of the fracture surface area for all the samples shows the defect-like crack, thread-like structure and slightly agglomeration as it has non-homogenous and poor dispersion in the sample. The CNTs filler tend to agglomerate due to their strong intrinsic van der Waals attraction and large aspect ratio, both PET/CNTs 0.1wt.% and 0.5wt.% primarily occur as randomly aggregated entanglements (Alexiou et al., 2020). It is also impossible to achieve a good dispersion nano-filler in the morphology surface even if the filler is in the nano size and should be easy to disperse in composite (Chatterjee et al., 2011).

In addition, the aggregate size exceeds, and the production of aggregates begins at concentrations over 0.4wt %, which could result in a reduction in the surface area of the MWCNTs-PET interface. Hence, the dispersion for PET-CNTs 0.1wt.% have better dispersion compared to the PET nanocomposite with 0.5wt.% nanofiller.

4.4 EMI Shielding Effectiveness

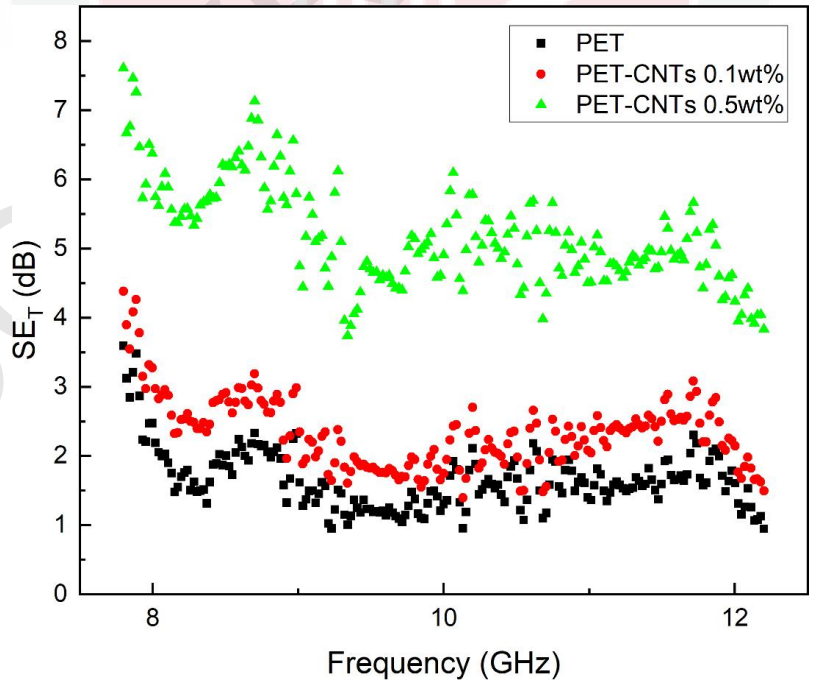

Figure 4.6 Total shielding effectiveness properties of pure PET and PET-CNTs 0.1 wt% and PET-CNTs 0.5wt%.

The overall EMI shielding effectiveness was calculated on the principle of the S-parameters as followed by Equation (8). In Figure 4.6 the EMI SE of PET, PET-CNTs 0.1wt.%, and PET-CNTs 0.5 wt. % nanocomposites were plotted as a function of nanofiller content in the χ-band frequency range for 1.6 mm thick plates. The samples were cut into rectangle bulk with dimension 40 × 18.9 mm. The EMI SE of most nanocomposites was found to be marginally dependent or even independent of frequency, and this behavior has been observed in a variety of polymer nanocomposites (Al-Saleh et al., 2013). For example, the maximum and minimum EMI SE values reported in this analysis throughout the χ-band frequency range were 7.607 dB and 3.735 dB, respectively, for the polymer nanocomposite with 0.5 wt % filler. As we can see the pattern of all the samples look alike but have different values of total shielding effectiveness. As illustrated in Fig. 4.6 the EMI SE versus frequency curves for all nanocomposite samples exhibited wave-like behavior. A similar pattern in ethylene-methyl-acrylate/carbon nanotubes nanocomposites and attributed it to the irregularity of the conductive network (Al-Saleh et al., 2013).

The polymer matrix sample with lower nano-filler 0.1wt.% has a slightly ascending SE_T pattern compared to pure PET sample because of the existence of the CNTs nano-filler that improves the SE_T of the polymer matrix. It is highly proven when the CNTs nano-filler increase to 0.5wt.% brings the escalate of the SE_T value. These findings are in line with previous research, which found that CNTs have higher permittivity values than pure PET with both real and imaginary parts, thus revealing better absorbing properties (Lim, 2017). Hence, the EMI SE increases as the nanofiller content increases for the same nanocomposite and shows that CNT-based materials have a better EMI shielding capability than pure polymer materials

especially for absorption properties (Al-Saleh et al., 2013). Moreover, it also can be related with the surface morphology which have been mentioned before, it shows that the good dispersion of morphology structure improves the connection network to give high SE_T value. For example, in PET-CNTs 0.1wt% have better dispersion structure and tend to give high SE_T value while in 0.5wt% nano-filler have poor dispersion but have the high SE_T value because of the function of the loaded contain, wt.%.

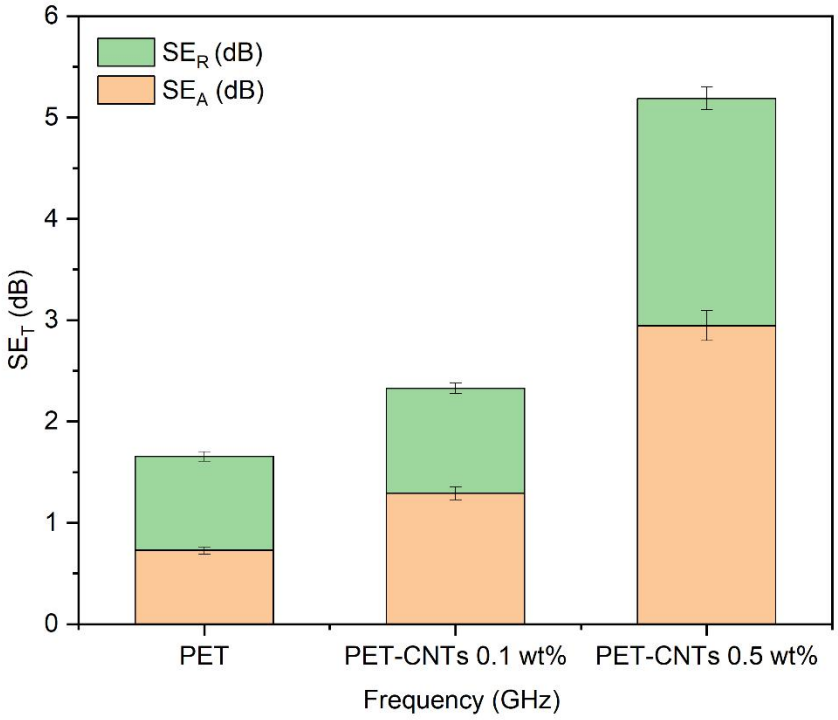

Figure 4.7: Figure illustrate the properties of the EMI shielding effectiveness which consist of absorbance loss and reflection loss.

Three main mechanisms attenuate EMI: reflection, absorption, and multiple reflections (Al-Saleh, 2015). We discovered that the contribution of absorption loss to overall shielding is larger than the contribution of reflection loss in prior work. Many researchers have reported similar findings for various nanocomposite materials (Al-Saleh et al., 2013). Figure 4.7 displays the properties of the EMI shielding

effectiveness (SE_T) value for each sample and was also discovered in this study that absorption loss (SE_A) was greater than reflection loss (SE_R). The absorption loss accounts for approximately 44 %, 56 % and 57 % of the overall EMI SE for pure PET, PET-CNTs 0.1w.t% and 0.5wt.% respectively that can be refer in Figure 4.7 as an example. The S-parameters received from the vector network analyzer were used to determine total shielding (SE_T), absorption loss (SE_A), and reflection loss (SE_R) as follows by the Equation (6)(7) and (8).

Absorption loss is greater than reflection loss, regardless of the CNT loading in the sample (Al-Saleh et al., 2013). For example, absorption loss is 1.292dB for the 0.1wt% of PET-CNTs nanocomposite compared to reflection loss is 1.035 dB and giving an overall EMI SE of 2.327 dB. PET-CNTs with 0.1wt.% have slightly ascending SE_T value compared to pure PET around 1.655 dB but PET nanocomposite illustrates the acceleration in SE_A region. PET-CNTs 0.5wt.% show a significant increase in SE_A value with 2.946 dB compared to polymer nanocomposite with lower filler and pure PET with 1.292 dB and 0.728 dB respectively. The reflection shielding effectiveness (SE_R) represented by yellow bars for PET-CNTs 0.5wt% show value of 2.241 dB followed by 1.035 dB and 0.927 dB for PET with 0.1wt% CNTs nano-filler and pure PET respectively. The value of SE_A shows an ascending pattern when the CNTs nano-filler were added to the polymer. Neat PET has higher SE_R value compared to the SE_A, nevertheless the SE_A value increases when the CNTs nano-filler were added and gives the higher value in SE_A more than SE_R in PET nanocomposite.

Table 4.1 Total shielding effectiveness value, absorption loss and reflection loss value for PET and PET-CNTs nanocomposite.

Samples	SE_A *(dB)*	±Error	SE_R *(dB)*	±Error	SE_T *(dB)*
PET	0.728	0.036	0.927	0.46	1.655
PET/CNTs 0.1 wt%	1.292	0.065	1.035	0.052	2.327
PET/CNTs 0.5 wt %	2.946	0.147	2.241	0.112	5.187

The absorbance properties for polymer nanocomposite are influenced by the permittivity value of the CNT nano-filler. Thus, the reflection properties of these samples contribute to the conductivity properties. Hence, it proves that these polymer matrices are more influenced by the permittivity compared to the conductivity as the absorbance loss is higher than the reflection loss. Choudhary et al. further stated that carbon nanotubes have the potential to be used to build lightweight and mechanically strong EMI shielding materials because CNTs have a low percolation threshold and a low loading level so that the bulk physical properties of the polymer matrix are not disturbed and provide any harmful effect on the mechanical properties of the resulting nanocomposites. In addition, it may be deduced from the data that these PET-CNTs nanocomposite have significant intrinsic absorption capabilities. However, because reflection occurs before absorption, the incident wave is reflected in its entirety (Al-Saleh et al., 2013). As a result, nanocomposites are currently unsuitable for applications needing low power reflection magnitude.

4.5 Electrical Conductivity

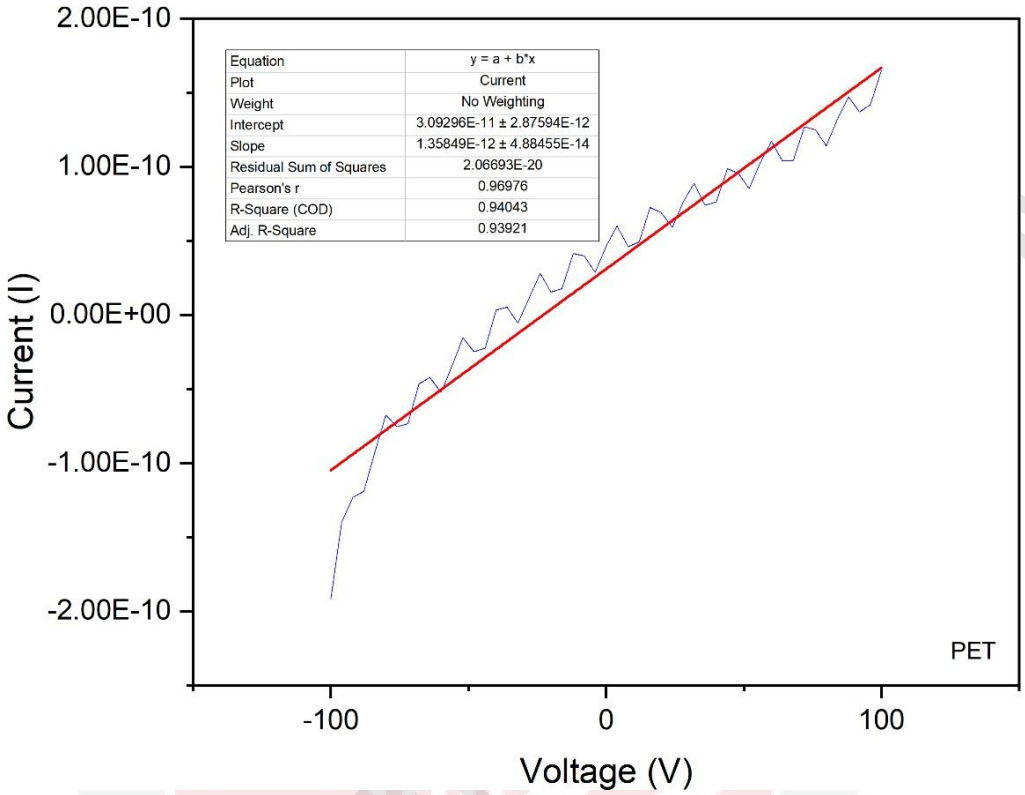

Figure 4.8: Electrical conductance of pure PET.

Figure 4.8 depicts the electrical conductance, S of the pure PET which is recognized for being a good electrical insulator among the polyesters. PET has been claimed to have a conductivity of 1×10^{-18} S/cm (Cruz-Delgado et al., 2014), which corresponds to an insulating material. The PET sample analyzed at different weight percent nano-fillers. For a pure PET sample, an ascending zig-zag pattern indicates the insulator pattern in the polymer and the slope value expresses the conductance of PET around 1.35849×10^{-12} S. The width, thickness, and length of the measured segments of PET and PET-CNTs nanocomposite bulk were measured by vernier caliper. All the parameters were set as constant of all samples with 40 mm × 18.9 mm, and thickness around 0.16mm. The value of the conductance can be found in the V vs I graph as

the slope value by using Equation (4). The calculated conductivity value for pure PET is 1.797×10^{-11} S/cm which means it has good electrical insulator properties.

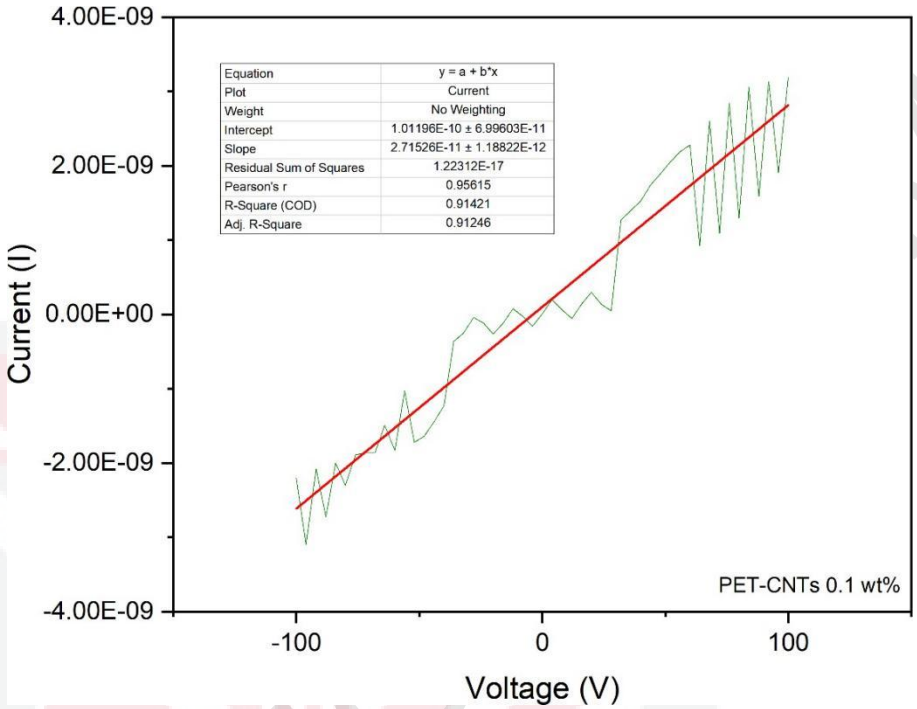

(a) PET-CNTs 0.1 wt.%

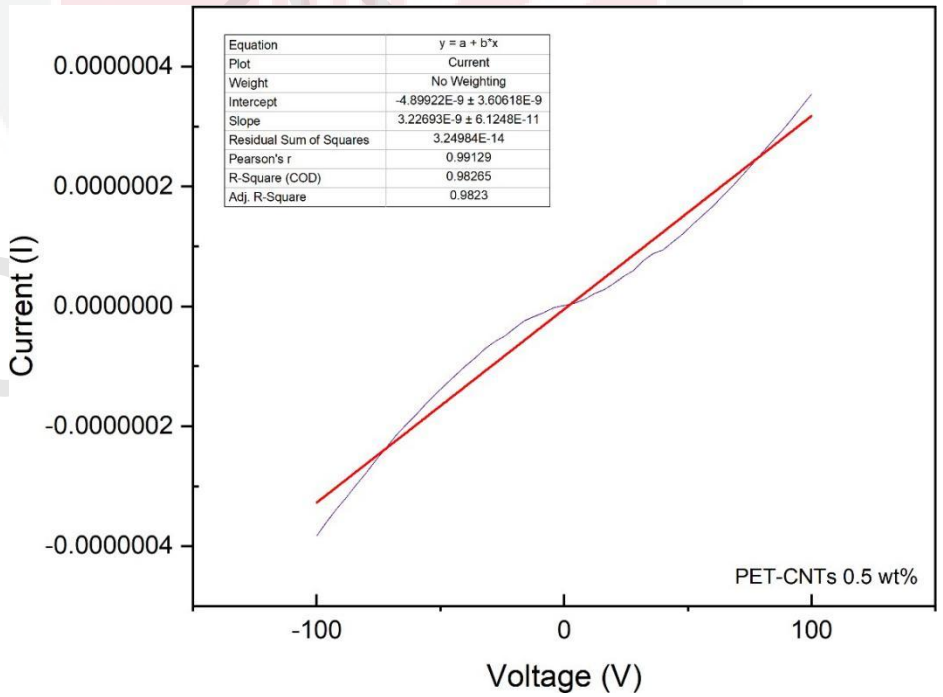

(b) PET-CNTs 0.5 wt.%

(c)

Figure 4.9 (a)(b): Electrical conductance of PET-CNTs 0.1 wt.% and PET-CNTs 0.5 wt.%.

Figure 4.9 shows the electrical conductance value, S of two different PET/CNT nanocomposites as a function of the nano-filler wt.% respectively. Insulating PET became electrically conductive with the addition of low amounts of CNTs, 0.1wt.%. When nanocomposite samples containing 0.1 wt.% CNTs were compared to electrical conductivity of neat PET, the electrical conductivity of the nanocomposites increased by ten orders of magnitude. The values for this sample were in the range of 10^{-10} (S/cm). The nanocomposite samples containing 0.5 wt.% of CNTs, on the other hand, showed a significant increase of 8 orders of magnitude in σ compared to the value of neat PET. The conductivity values for PET-CNTs nanocomposite with 0.1 wt.% and 0.5 wt.% are 3.5915×10^{-10} S/cm and 4.2684×10^{-8} S/cm respectively. Hence, when the wt.% of nano-filler was increased, the electrical conductivity tended to rise.

Table 4.2 Parameter for conductance, resistance, conductivity, and resistivity of the neat PET and PET-CNTs nanocomposite.

Samples	**Conductance, *S***	**Resistance, *Ω***	**Conductivity, *S/cm***	**Resistivity, *Ω.cm***
PET	1.3585×10^{-12}	7.3638×10^{11}	1.7970×10^{-11}	5.5648×10^{10}
PET/CNTs 0.1 wt%	2.7152×10^{-11}	$3.6830\times 10^{\wedge 10}$	3.5915×10^{-10}	2.7844×10^{9}
PET/CNTs 0.5 wt %	3.2270×10^{-9}	$3.0990\times 10^{\wedge 8}$	4.2684×10^{-8}	2.3428×10^{7}

The conductivity of the sample more conductive as the loading of CNTs filler increases as shown in Table 4.2. The increase in conductivity can be proven when the total shielding effectiveness, SE_T of the sample is also increasing. The conductivity influences the SE_R value and it shows that when the conductivity increases in PET nanocomposite, the SE_R also tend to increase as in Table 4.2. Furthermore, when the nano-filler loaded increase, there is more connection network in this sample that allow the sample to conduct current. For example, the PET-CNTs nanocomposite of 0.5 wt.% more conductive than 0.1 wt.% sample and shows that the SE_T of the sample increasing with higher nano-filler. The dispersion of the sample also can affect the conductivity. In good dispersion and homogenous sample, the network CNTs linking together, and the connection will be more effective to give good conductivity value hence high in SE_T value. As refer to the Figure in 4.2 (b) for 0.1wt.%, the dispersion of the samples is homogenous, and it influence the CNTs network connection to conduct current effectively. For 0.5 wt.% nanocomposite, it contains poor dispersion but have high nano-filler value which can be good network to conductivity. Thus, that is the reason why the conductivity value increasing at good distribution sample as increase of the function of nano-filler contains. The finding also similar with the previous study where the addition of 1 wt.% CNTs leads to a significant increase in electrical conductivity, almost fifteen orders of magnitude greater than the pure PET value (Larciprete et al., 2019) Nanocomposite samples containing 1% wt CNTs had an average electrical conductivity enhancement of nine orders of magnitude when compared with pure PET samples (Cruz-Delgado et al., 2014).

CHAPTER 5: CONCLUSION

5.1 Conclusion

In this study, polymer nanocomposites with different functions of composition are successfully fabricated by using Polyethylene Terephthalate (PET) as the polymer matrix and Carbon Nanotubes (CNTs) as the nano-filler. The fabrication of the sample using the melt blending and injection molding method.

The XRD pattern of pure PET and PET-CNTs nanocomposite samples are nearly unchanged since the XRD peaks of pure PET are too high and overshadow the filler's peak. However, CNTs nano-fillers with a high wt% content, have more intense semi-crystalline peaks than neat PET. The composition of the filler directly proportional the crystallinity of the sample. FESEM analysis indicates that all the polymer nanocomposites samples are not evenly distributed, resulting in flaws such as cracks, thread-like structure, and aggregation are present.

Besides, PET and nanocomposite sample's electrical conductivity is interpreted by a Two-point Probe analysis. According to earlier research, increasing the CNTs nano-filler composition can improve electrical conductivity significantly because CNTs can produce a superior electrical conductivity because the conductive path is created more efficiently among the composites. The conductivity shows $3\times$ increasing in magnitude order from in PET-CNTs 0.5 wt% than the pure PET. The conductivity values are 3.2270×10^{-9} S/cm for PET-CNTs 0.5 wt% while 2.7152×10^{-11}S/cm and 1.3585×10^{-12} S/cm for PET-CNTs 0.1 wt% and pure PET respectively. Hence, CNTs have good electrical conductivity properties, which can affect the conductivity properties of PET-CNT nanocomposite.

Lastly, the EMI Shielding absorbance performance of the nanocomposites can be identified using VNA. According to the results and discussion in the preceding chapter, EMI shielding can increase when the carbon nano-filler composition in polymer nanocomposites increases. The total SE value ascending from pure PET to PET with higher filler with 1.655, 2.375 and 5.187. The total EMI shielding effectiveness, SE increased significantly with improvement of 313 % in PET-CNTs 0.5 wt% while PET-CNTs 0.1 wt% with 140% increment. The PET-CNTs nanocomposite has better absorption capabilities than reflection properties with the maximum permittivity value compared to neat PET.

5.2 Suggestions

The nano-filler content has a significant impact on the nanocomposites' characteristics. The loading amount of carbon nano-fillers should be increased to 1 wt.% to examine more composition modifications and their impact on characteristics. Another form of polymer matrix, such as polystyrene, is also preferred since it successfully demonstrates EMI absorption behavior and better electrical properties. Hence, we may explore the efficacy of carbon nano-fillers within this matrix material.

Furthermore, additional work might be encouraged using various fabrication techniques to compare a wide variety of melt blending processes, such as extrusion, solution casting, and others, to evaluate the efficacy of dispersion inside polymer nanocomposites. Melt compounding is a process that results in a more uniform dispersion and distribution of MWCNTs within the PET matrix, but it has brittle characteristic than using direct extrusion which made the polymer stiffer. Melt compounding the PET-CNTs polymer leading up to extrusion is recommended to enhance the composites' mechanical and electrical properties (Rodríguez et al., 2013).

REFERENCES

Advanced materials for electromagnetic shielding. (2018). https://doi.org/10.1002/9781119128625

Alexiou, V. F., Mathioudakis, G. N., Andrikopoulos, K. S., Soto Beobide, A., & Voyiatzis, G. A. (2020). Poly(ethylene terephthalate) carbon-based nanocomposites: A crystallization and molecular orientation study. *Polymers,12*(11), 2626. https://doi.org/10.3390/polym12112626

Al-Saleh, M. H. (2015). Influence of conductive network structure on the EMI shielding and electrical percolation of carbon nanotube/polymer nanocomposites. *Synthetic Metals, 205*, 78–84. https://doi.org/10.1016/j.synthmet.2015.03.032

Al-Saleh, M. H., Saadeh, W. H., & Sundararaj, U. (2013). EMI shielding effectiveness of carbon based nanostructured polymeric materials: A comparative study. *Carbon, 60,* 146–156. https://doi.org/10.1016/j.carbon.2013.04.008

Chen, I.-H., Wang, C.-C., & Chen, C.-Y. (2010). Fabrication and structural characterization of polyacrylonitrile and carbon nanofibers containing plasma- modified carbon nanotubes by electrospinning. *The Journal of Physical Chemistry C, 114*(32), 13532–13539. https://doi.org/10.1021/jp103993b

Choudhary, V., & Gupt, A. (2011). Polymer/Carbon Nanotube Nanocomposites. *Carbon Nanotubes - Polymer Nanocomposites.* https://doi.org/10.5772/18423

Cruz-Delgado, V. J., Ávila-Orta, C. A., Espinoza-Martínez, A. B., Mata-Padilla, J. M., Solis-Rosales, S. G., Jalbout, A. F., Medellín-Rodríguez, F. J., & Hsiao, B. S. (2014). Carbon nanotube surface-induced crystallization of polyethylene terephthalate (PET). *Polymer, 55*(2), 642–650. https://doi.org/10.1016/j.polymer.2013.12.029

Demirel, B., Yaras, A., & Elçiçek, H. (2011). Crystallization Behavior of PET Materials Norizan, M. N., Moklis, M. H., Ngah Demon, S. Z., Halim, N. A., Samsuri, A.,

Dupaix, R.B. (2003). Temperature and rate dependent finite strain behavior of poly(ethylene terephthalate) and poly(ethylene terephthalate)-glycol above the glass transition temperature.

Fiber-Reinforced Polymer composite (FRP). (2021). [Image]. Https://Romeorim.Com/What-Are-Composites/. https://romeorim.com/wpcontent/uploads/2018/07/FiberMatrixComposite3.png

González, M., Mokry, G., de Nicolás, M., Baselga, J., & Pozuelo, J. (2016). Carbon nanotube composites as electromagnetic shielding materials in GHz 62 Range.

Gupta, S., & Tai, N.-H. (2019). Carbon materials and their composites for electromagnetic interference shielding effectiveness in X-band. *Carbon, 152*,159–187. https://doi.org/10.1016/j.carbon.2019.06.002

G. Santoro, M. A. Gómez, C. Marco, and G. Ellis, "A solvent-free dispersion method for the preparation of PET/MWCNT composites," *Macromolecular Materials and Engineering*, vol. 295, no. 7, pp. 652–659, 2010.

H. Haddad, H., Masood, S., & Erbulut, D. U. (2009). A study of blow moulding simulation and structural analysis for PET bottles. *Australian Journal of Mechanical Engineering, 7*(1), 69–76. https://doi.org/10.1080/14484846.2009.11464580

Henry, D., Eby, N., Goodge, J., & Mogk, D. (2016, November 10). *X-ray reflection in accordance with Bragg's Law*. Geochemical Instrumentation and Analysis. Retrieved February 5, 2022, from https://serc.carleton.edu/research_education/geochemsheets/BraggsLaw.html.

ism waste & recycling, 2021. *PET.* [image] Available at: <https:ismwaste.co.uk/images/help/plastic1-pet.jpg>[Accessed 5 February 2022].

Jaroszewski, M. W., Thomas, S., & Rane, A. V. (2019). *Advanced materials for electromagnetic shielding: Fundamentals, properties, and applications.* JohnWiley & Sons Inc.

Jeon IY, Baek JB (2010) Nanocomposites derived from polymers and inorganic nanoparticles. Materials 3:3654–3674

Ji, L. N. (2013). Study on Preparation Process and Properties of Polyethylene Terephthalate (PET). *Applied Mechanics and Materials, 312*, 406–410. https://doi.org/10.4028/www.scientific.net/amm.312.406

Joshi, A., & Datar, S. (2015). Carbon nanostructure composite for electromagnetic interference shielding. *Pramana, 84*(6), 1099–1116. https://doi.org/10.1007/s12043-015-1005-9

J. Y. Kim, H. S. Park, and S. H. Kim, "," *Journal of Applied Polymer Science*, vol. 103, no. 3, pp. 1450–1457, 2007.

Kamigaito, O. (1991). What can be improved by nanometer composites? *Journal of the Japan Society of Powder and Powder Metallurgy, 38*(3), 315–321. https://doi.org/10.2497/jjspm.38.315

Karimi, P., Ostoja-Starzewski, M., & Jasiuk, I. (2016). Experimental and computational study of shielding effectiveness of polycarbonate carbon

nanocomposites. *Journal of Applied Physics, 120*(14), 145103. 63 https://doi.org/10.1063/1.4964691

Kolanowska, A., Janas, D., Herman, A. P., Jędrysiak, R. G., Giżewski, T., & Boncel, S. (2018). From blackness to invisibility – carbon nanotubes role in the attenuation of and shielding from radio waves for stealth technology. *Carbon, 126*, 31– 52. https://doi.org/10.1016/j.carbon.2017.09.078

Larciprete, M. C., Paoloni, S., Orazi, N., Mercuri, F., Orth, M., Gloy, Y., Centini, M., Li Voti, R., & Sibilia, C. (2019). Infrared emissivity characterization of carbon nanotubes dispersed poly(ethylene terephthalate) fibers. International Journal of Thermal Sciences, 146, 106109. https://doi.org/10.1016/j.ijthermalsci.2019.106109

Lataste, J.-F. (2010). Electrical resistivity for the evaluation of reinforced concrete structures. *Non-Destructive Evaluation of Reinforced Concrete Structures*, 243–275. https://doi.org/10.1533/9781845699604.2.243

Lee, S.-S., & Yee, A. F. (2003). Temperature-Dependent Transition of Deformation Mode in Poly(1,4-cyclohexylenedimethylene terephthalate)/Poly(ethylene terephthalate) Copolymers. *Macromolecules, 36*(18), 6791–6796. https://doi.org/10.1021/ma034660a

Mai, Y. W., & Yu, Z.-Z. (2007). Polymer nanocomposites. Woodhead Publishing.

Mallakpour, S., & Behranvand, V. (2017). Application of recycled PET/carboxylated multi-walled carbon nanotube composites for Cd2 adsorption from aqueous solution: a study of morphology, thermal stability, and electrical conductivity. *Colloid and Polymer Science, 295*(3), 453–462. https://doi.org/10.1007/s00396- 017-4022-z

Metrohm, 2021. *Molecular structure of linear PET*.. [image] Available at: [Accessed 5 February 2022].

Mohamad, I. S., Knight, V. F., & Abdullah, N. (2020). Carbon nanotubes: functionalisation and their application in chemical sensors. RSC Advances, 10(71), 43704–43732. https://doi.org/10.1039/d0ra09438b

Mohammed, J., Tchouank Tekou Carol, T., Hafeez, H. Y., Basandrai, D., Bhadu, G. R., Godara, S. K., Narang, S. B., & Srivastava, A. K. (2019). Electromagnetic interference (EMI) shielding, microwave absorption, and optical sensing properties of BAM/CCTO Composites in ku-band. *Results in Physics, 13*, 102307. https://doi.org/10.1016/j.rinp.209.102307

Norizan, M. N., Moklis, M. H., Ngah Demon, S. Z., Halim, N. A., Samsuri, A., Mohamad, I. S., Knight, V. F., & Abdullah, N. (2020). Carbon nanotubes: functionalisation and their application in chemical sensors. *RSC Advances, 10*(71), 43704–43732. https://doi.org/10.1039/d0ra09438b 64

Rane, A. V., Kanny, K., Abitha, V. K., & Thomas, S. (2018, June 22). *Methods for Synthesis of Nanoparticles and Fabrication of Nanocomposites*. Synthesis

of Inorganic Nanomaterials. http:/www.sciencedirect.com/science/article/pi I/B97800810197570005

Rodríguez-Uicab, O., May-Pat, A., Avilés, F., Toro, P., & Yazdani-Pedram, M. (2013). Influence of Processing Method on the Mechanical and Electrical Properties of MWCNT/PET Composites. *Journal of Materials, 2013*, 1–10. https://doi.org/10.1155/2013/656372

Rodriguez, F., Cohen, F., Ober, C. K., & Archer, L. (2003). Principles of Polymer Systems. https://doi.org/10.1201/b12837

Sotiropoulos, A., Koulouridis, S., Masouras, A., Kostopoulos, V., & Anastassiu, H. T. (2021). Carbon nanotubes films in glass fiber polymer matrix forming structures with high absorption and shielding performance in X-Band. *Composites Part B: Engineering, 217*, 108896. https://doi.org/10.1016/j.compositesb.2021.108896

S.H. Masood, V. S. (2006). Design and Development of Large Collapsible PET Water Cooler Bottles. *International Conference on Computer Graphics, Imaging and Visualisation (CGIV'06)*. https://doi.org/10.1109/cgiv.2006.35

Vargas-Bernal, R. (2015). Performance analysis of electromagnetic interference shielding based on carbon nanomaterials used in AMS/RF IC Design. *Advances in Computer and Electrical Engineering,* 268–294. https://doi.org/10.4018/978-1-4666-6627-6.ch011

Visakh, P. M. (2015). Polyethylene Terephthalate: Blends, Composites, and Nanocomposites – State of Art, New Challenges, and Opportunities. *Poly(Ethylene Terephthalate) Based Blends, Composites and Nanocomposites,* 1–14. https://doi.org/10.1016/b978-0-323-31306-3.00001-4

Wang, D., Liu, Q., Wang, Y., Li, M., Liu, K., Chen, J., & Qing, X. (2015). Reinforcement of polyethylene terephthalate via addition of carbon-based materials. *Poly(Ethylene Terephthalate) Based Blends, Composites and Nanocomposites,* 41–64. https://doi.org/10.1016/b978-0-323-31306-3.00003-8

Z. Zhu, R. Wang, Z. Dong, X. Huang, and D. Zhang, "Morphology, crystallization, and mechanical properties of poly(ethylene terephthalate)/multiwalled carbon nanotubes composites," *Journal of Applied Polymer Science*, vol. 120, no. 6, pp. 3460–3468, 2011

APPENDICES

Vector Network Analyzer

For pure PET, at frequency 8.35 Hz, S_{11}=0.4501,

S_{21}= 0.8402Shielding Absorbance, SE_A

$$SE_A = 10\,log\,(\frac{1-|s_{11}|^2}{|s_{21}|^2})$$

$$SE_A = 10\,log\,(\frac{1-|0.4501|^2}{|0.8402|^2})$$

$$SE_A = 10\,log(1.12958)$$

SE_A= 0.5292

Shielding Reflection, SE_R

$$SE_R = 10\,log\,(\frac{1}{1-|s_{11}|^2})$$

$$SE_R = 10\,log\,(\frac{1}{1-|0.4501|^2})$$

$$SE_R = 10\,log(1.2541)$$

SE_R= 0.9832

Total average of at each frequency, SE_A= 0.7283,

SE_R= 0.9275

Total Shielding Effectiveness, SE_T

$SE_T = SE_A + SE_R$

SE_T = 0.7283 +0.9275

SE_T = 1.6558

Conductivity

$$\sigma = \frac{I}{V} \cdot \frac{L}{w \cdot t}$$

PET,

From slope, C= $\frac{I}{V} = 1.3585 \times 10^{-12}$ S

$$\sigma = 1.3585 \times 10^{-12} \cdot \left(\frac{4 \text{ cm}}{1.89 \text{ cm} - 0.16 \text{ cm}} \right)$$

$$\sigma = 1.3585 \times 10^{-12} (13.2275 \text{ cm})$$

$$\sigma = 1.7970 \times 10^{-11} \text{S/cm}$$

Resistivity,

$$\rho = \frac{1}{\sigma}$$

$$\rho = \frac{1}{1.7970 \times 10^{-11} \text{S/cm}}$$

$$\rho = 5.5648 \times 10^{10}$$

PET-CNTs 0.1 wt%

From slope, C= $\frac{I}{V} = 2.7153 \times 10^{-11} S$

$$\sigma = 2.7153 \times 10^{-11} \cdot \left(\frac{4 \text{ cm}}{1.89 \text{ cm} - 0.16 \text{ cm}} \right)$$

$$\sigma = 2.7153 \times 10^{-11} (13.2275 \text{ cm})$$

$$\sigma = 3.5915 \times 10^{-10} \text{S/cm}$$

Resistivity,

$$\rho = \frac{1}{\sigma}$$

$$\rho = \frac{1}{3.5915 \times 10^{-10} \text{S/cm}}$$

$$\rho = 2.7844 \times 10^{9}$$

PET-CNTs 0.5 wt%

From slope, $C = \frac{I}{V} = 3.2270 \times 10^{-11} S$

$$\sigma = 3.2270 \times 10^{-11} \cdot \left(\frac{4 \text{ cm}}{1.89 \text{ cm} - 0.16 \text{ cm}} \right)$$

$$\sigma = 3.2270 \times 10^{-11} (13.2275 \text{ cm})$$

$$\sigma = 4.2684 \times 10^{-8} \text{S/cm}$$

Resistivity,

$$\rho = \frac{1}{\sigma}$$

$$\rho = \frac{1}{4.2684 \times 10^{-8} \text{S/cm}}$$

$$\rho = 2.3428 \times 10^{7}$$

PET

Name and formula

Reference code:	98-001-7130
Mineral name:	Graphite 2H
Compound name:	Graphite 2H
Chemical name:	Carbon
Common name:	Graphite 2H
ICSD name:	Carbon
Chemical formula:	C_1
Second chemical formula:	C

Crystallographic parameters

Crystal system:	Hexagonal
Space group:	P 63 m c
Space group number:	186
a (Å):	2.4700
b (Å):	2.4700
c (Å):	6.7900
Alpha (°):	90.0000
Beta (°):	90.0000
Gamma (°):	120.0000
Calculated density (g/cm^3):	2.22
Measured density (g/cm^3):	2.16
Volume of cell (10^6 pm^3):	35.88
Z:	4.00
RIR:	2.41

Subfiles and quality

Subfiles:	ICSD Pattern Inorganic Mineral
Quality:	Calculated (C)

Comments

ICSD collection code:	31170
Creation Date:	1/1/1970
Modification Date:	1/1/1970
Calculated Pattern Original Remarks:	Compound with mineral name:
Original ICSD space group:	P63MC
ICSD Collection Code:	31170
Original ICSD space group:	P63MC

Theoretically calculated cell from 3rd ref (Fayos): 2.461, 6.708

At least one temperature factor missing in the paper.

No R value given in the paper

Unusual difference between calculated and measured density
X-ray diffraction from single crystal
The structure has been assigned a PDF number (experimental powder diffraction data): 42-1487

The structure has been assigned a PDF number (calculated powder

diffraction data): 01-075-1621

Compound with mineral name: Graphite 2H

Recording date: 1/1/1980

Modification date: 4/1/2006

Mineral origin: Graphite 2H - from Kropfmuehl, Bavaria

ANX formula: N

Z: 4

Authors density: 2.16

Calculated density: 2.22

Pearson code: hP4

Wyckoff code: b a

PDF code: 00-042-1487

Publ. title: Ueber die Kristallstruktur des Graphits.

References

Primary reference: Hassel, O., *Journal of Solid State Chemistry*, **148**, 278, (1999)

Peak list

No.	h	k	l	d [A]	2Theta[deg]	I [%]
1	0	0	2	3.39500	26.228	100.0
2	0	1	0	2.13908	42.214	3.2
3	0	1	1	2.04023	44.365	15.5

4	0	1	2	1.80980	50.381	3.4
5	0	0	4	1.69750	53.974	6.3
6	0	1	3	1.55463	59.404	4.9
7	0	1	4	1.32969	70.804	0.9
8	1	1	0	1.23500	77.177	4.7
9	1	1	2	1.16060	83.167	7.8
10	0	1	5	1.14648	84.425	1.4
11	0	0	6	1.13167	85.793	1.1

Structure

No.	Name	Elem.	X	Y	Z	Biso	sof	Wyck.
1	C1	C	0.33330	0.66670	0.00500	0.5000	1.0000	2b
2	C2	C	0.00000	0.00000	0.00000	0.5000	1.0000	2a

Stick Pattern

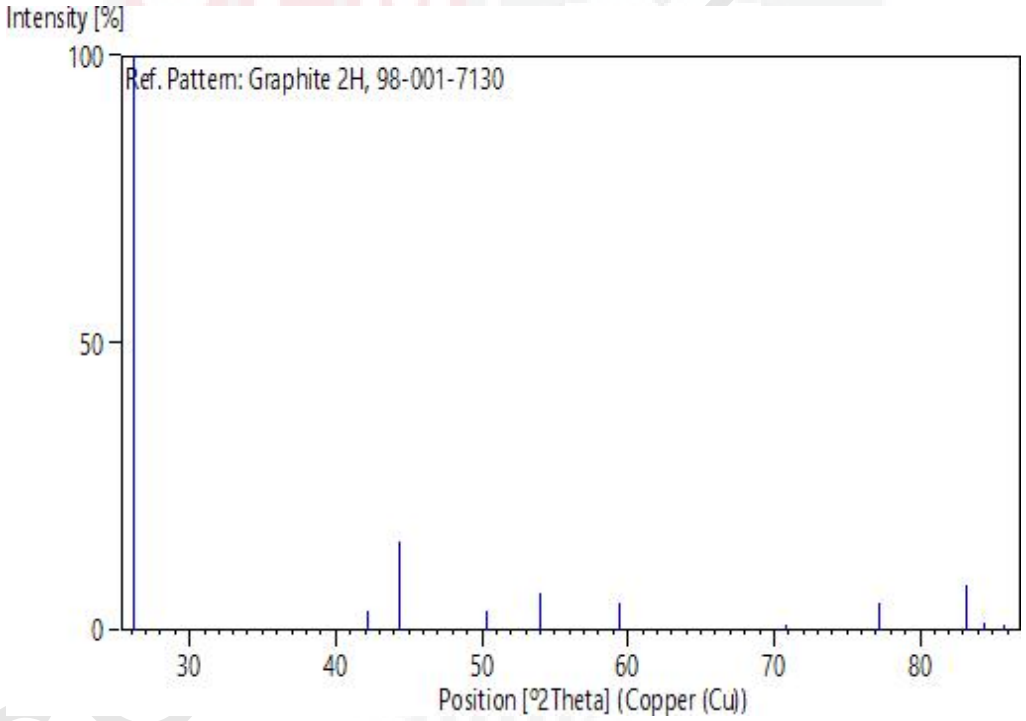

PET-CNTs 0.1 wt%

Name and formula

Reference code:	98-006-2711
Mineral name:	Graphite 2H
Compound name:	Graphite 2H
Chemical name:	Carbon
Common name:	Graphite 2H
ICSD name:	Carbon
Chemical formula:	C_1
Second chemical formula:	C

Crystallographic parameters

Crystal system:	Hexagonal
Space group:	P 63/m m c
Space group number:	194
a (Å):	2.4700
b (Å):	2.4700
c (Å):	6.8000
Alpha (°):	90.0000
Beta (°):	90.0000
Gamma (°):	120.0000
Calculated density (g/cm^3):	2.22
Volume of cell (10^6 pm^3):	35.93
Z:	4.00
RIR:	2.29

Subfiles and quality

Subfiles:	ICSD Pattern Inorganic Mineral
Quality:	Calculated (C)

Comments

ICSD collection code:	53781
Creation Date:	1/1/1970
Modification Date:	1/1/1970
Calculated Pattern Original Remarks:	Compound with mineral name:
Structures:	Graphite(2H)
Original ICSD space group:	P63/MMC
ICSD Collection Code:	53781

Original ICSD space group: P63/MMC

AE: C1,2: C3

Cell from 2nd reference: 2.47, 6.75, from 3rd ref.: 2.47, 6.80

At least one temperature factor missing in the paper.

No R value given in the paper.

X-ray diffraction (powder)

Structure type : Graphite(2H)

Structure type prototype : Graphite(2H)

The structure has been assigned a PDF number (experimental powder

diffraction data): 41-1487

The structure has been assigned a PDF number (calculated powder

diffraction data): 01-071-4630

Compound with mineral name: Graphite 2H

Structure type: Graphite(2H)

Recording date: 4/1/2003

Modification date: 8/1/2008

Mineral origin: Graphite 2H - natural

ANX formula: N

Z: 4

Calculated density: 2.22

Pearson code: hP4

Wyckoff code: c b

PDF code: 00-041-1487

Publ. title: Structure of graphite

References

Primary reference: Hull, A.W., *Berichte der Deutschen Chemischen Gesellschaft*, **59**, 2433, (1926)

Peak list

No.	h	k	l	d [A]	2Theta[deg]	I [%]
1	0	0	2	3.40000	26.189	100.0
2	0	1	0	2.13908	42.214	3.4
3	0	1	1	2.04050	44.358	16.6
4	0	1	2	1.81056	50.358	3.3
5	0	0	4	1.70000	53.888	6.9
6	0	1	3	1.55571	59.358	5.0
7	0	1	4	1.33089	70.730	0.8
8	1	1	0	1.23500	77.177	5.0
9	1	1	2	1.16079	83.150	8.0
10	0	1	5	1.14768	84.316	1.4
11	0	0	6	1.13333	85.637	1.3

Structure

No.	Name	Elem.	X	Y	Z	Biso	sof	Wyck.
1	C1	C	0.33330	0.66670	0.25000	0.5000	1.0000	2c
2	C2	C	0.00000	0.00000	0.25000	0.5000	1.0000	2b

Stick Pattern

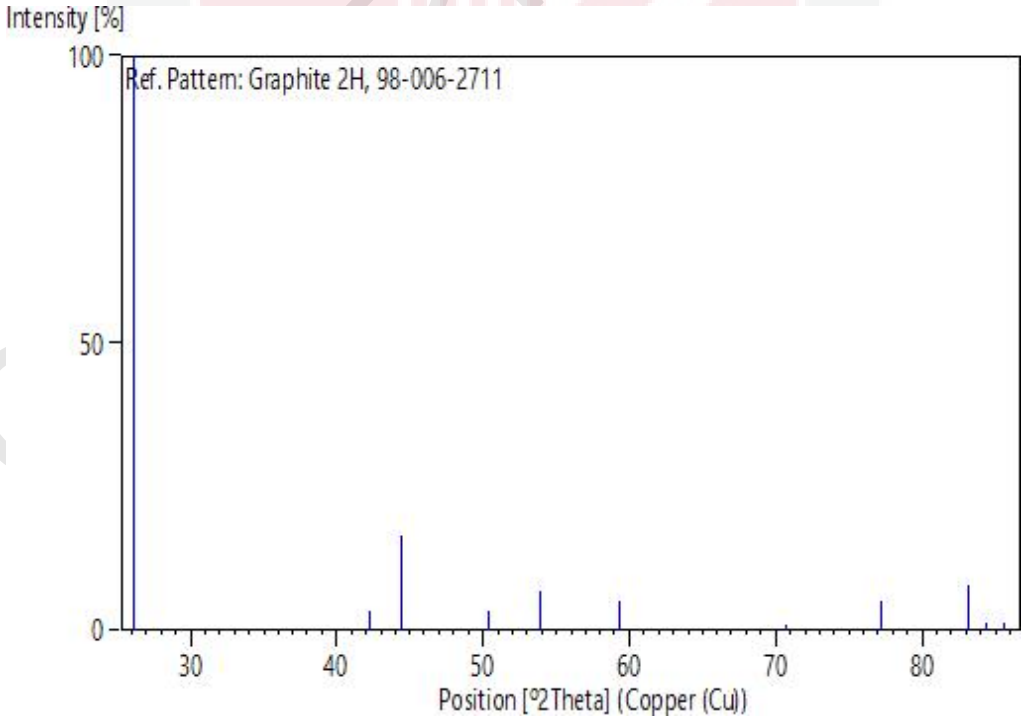

PET-CNTs 0.5 wt%

Name and formula

Reference code:	98-001-7130
Mineral name:	Graphite 2H
Compound name:	Graphite 2H
Chemical name:	Carbon
Common name:	Graphite 2H
ICSD name:	Carbon
Chemical formula:	C_1
Second chemical formula:	C

Crystallographic parameters

Crystal system:	Hexagonal
Space group:	P 63 m c
Space group number:	186
a (Å):	2.4700
b (Å):	2.4700
c (Å):	6.7900
Alpha (°):	90.0000
Beta (°):	90.0000
Gamma (°):	120.0000
Calculated density (g/cm^3):	2.22
Measured density (g/cm^3):	2.16
Volume of cell (10^6 pm^3):	35.88
Z:	4.00
RIR:	2.41

Subfiles and quality

Subfiles:	ICSD Pattern Inorganic Mineral
Quality:	Calculated (C)

Comments

ICSD collection code:	31170
Creation Date:	1/1/1970
Modification Date:	1/1/1970
Calculated Pattern Original Remarks:	Compound with mineral name:
Original ICSD space group:	P63MC
ICSD Collection Code:	31170
Original ICSD space group:	P63MC

Theoretically calculated cell from 3rd ref (Fayos): 2.461, 6.708

At least one temperature factor missing in the paper.

No R value given in the paper

Unusual difference between calculated and measured density
X-ray diffraction from single crystal
The structure has been assigned a PDF number (experimental powder diffraction data): 42-1487

The structure has been assigned a PDF number (calculated powder

diffraction data): 01-075-1621

Compound with mineral name: Graphite 2H

Recording date: 1/1/1980

Modification date: 4/1/2006

Mineral origin: Graphite 2H - from Kropfmuehl, Bavaria

ANX formula: N

Z: 4

Authors density: 2.16

Calculated density: 2.22

Pearson code: hP4

Wyckoff code: b a

PDF code: 00-042-1487

Publ. title: Ueber die Kristallstruktur des Graphits.

References

Primary reference: Hassel, O., *Journal of Solid State Chemistry*, **148**, 278, (1999)

Peak list

No.	h	k	l	d [A]	2Theta[deg]	I [%]
1	0	0	2	3.39500	26.228	100.0
2	0	1	0	2.13908	42.214	3.2
3	0	1	1	2.04023	44.365	15.5
4	0	1	2	1.80980	50.381	3.4

5	0	0	4	1.69750	53.974	6.3
6	0	1	3	1.55463	59.404	4.9
7	0	1	4	1.32969	70.804	0.9
8	1	1	0	1.23500	77.177	4.7
9	1	1	2	1.16060	83.167	7.8
10	0	1	5	1.14648	84.425	1.4
11	0	0	6	1.13167	85.793	1.1

Structure

No.	Name	Elem.	X	Y	Z	Biso	sof	Wyck.
1	C1	C	0.33330	0.66670	0.00500	0.5000	1.0000	2b
2	C2	C	0.00000	0.00000	0.00000	0.5000	1.0000	2a

Stick Pattern

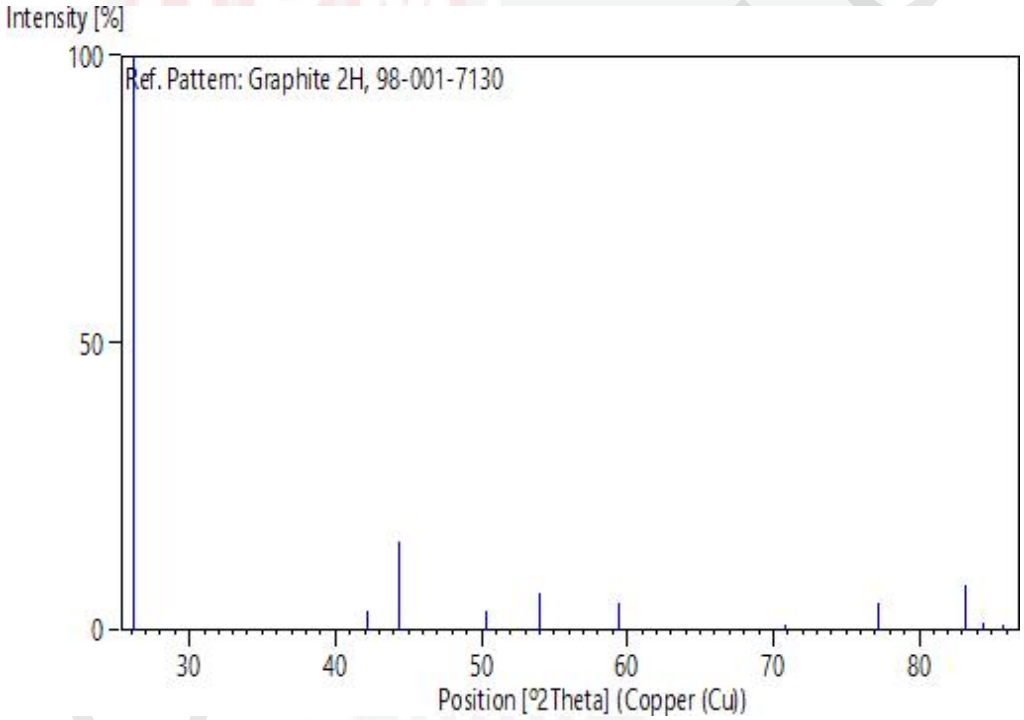

VITAE

Name	:	Nur Hamizah Binti Hashim
Address	:	No 21, Jalan 9/10, Perjiranan 9, Taman Air Biru, Pasir Gudang, Johor.
Telephone No.	:	017-764 7624
Email	:	nurhamizahbintihashi@gmail.com

Personal Info

Age	: 23	Religion	: Islam
Date of Birth	: 07 December 1999	Race	: Malay
Gender	: Female	Nationality	: Malaysian

Education

Bachelor

Field of Study	: Bachelor of Science in Material Science with Honours
Institution	: Universiti Putra Malaysia
Graduation Date	: Ongoing

Matriculation in Science

Institution	: Agricultural Science Foundation, UPM
Year	: 2017/2018

Sijil Pelajaran Malaysia (S.P.M)

School	: Sekolah Menengah Kebangsaan Pasir Gudang
Year	2016

Penilaian Menengah Rendah (P.M.R)

School	: Sekolah Menengah Kebangsaan Pasir Gudang
Year	2014